Supporting Information

Super-resolution imaging of antibody conjugated biodegradable periodic mesoporous organosilica nanoparticles for targeted chemotherapy of prostate cancer

Pradip Das,*[a,b] Silvia Pujals,*[c] Lamiaa M. A. Ali,[d] Magali Gary-Bobo,[d] Lorenzo Albertazzi,[b,e] Jean-Olivier Durand[a]

[a] Institute Charles Gerhardt Montpellier (ICGM), University of Montpellier, CNRS, ENSCM, Montpellier 34293, France. Email: daspradip43@gmail.com

[b] Nanoscopy for Nanomedicine Group, Institute for Bioengineering of Catalonia (IBEC), Barcelona 08036, Spain.

[c] Department of Biological Chemistry, Institute for Advanced Chemistry of Catalonia (IQAC-CSIC), Barcelona, Spain. Email: silvia.pujals@iqac.csic.es

[d] IBMM, University of Montpellier, CNRS, ENSCM, 34093 Montpellier, France.

[e] Department of Biomedical Engineering, Institute of Complex Molecular Systems (ICMS), Eindhoven University of Technology, Eindhoven, The Netherlands.

Experimental Section:

Chemicals and Materials. (3-Aminopropyl)triethoxysilane (99%) and triethylamine (≥99%) were purchased from Sigma-Aldrich. Cyanine 3 NHS ester and cyanine 5 NHS ester were obtained from Lumiprobe. Anhydrous dimethylformamide (99.8%) was purchased from Acros Organics. Cetyltrimethylammonium bromide (≥98%), sodium hydroxide (≥98%), and ammonium nitrate (≥98%) were bought from Sigma-Aldrich. 1,4-bis(triethoxysilyl)benzene (95%), 1,2-bis(triethoxysilyl)ethylene (95%) and bis(3-triethoxysilylpropyl)disulfide (90%) were purchased from abcr. In addition, bis(3-triethoxysilylpropyl)tetrasulfide (≥90%) was bought from Sigma-Aldrich. 9-Fluorenylmethyl carbazate (>98%) was purchased from Tokyo Chemical Industry (TCI). 3-(Triethoxysilyl)propyl isocyanate (95%) was purchased from Sigma-Aldrich. Fluorescamine and L-glutathione reduced (>98%) were purchased from Alfa Aesar. Sodium periodate (≥99.8%), 1-ethyl-3-(3-dimethylaminopropyl)carbodiimide

hydrochloride, N-hydroxysuccinimide (98%) were bought from Sigma-Aldrich. A recombinant anti-M6PR (cation independent) antibody was purchased from Abcam. PD-10 desalting columns packed with Sephadex G-25 resin was obtained from GE Healthcare. Superfrost microscope slides (26 x 76 x 1 mm) and coverslips (22 x 22 mm, # 1.5) were purchased from Epredia. Glucose (≥99.5%), cysteamine (≥98%), Glucose Oxidase from Aspergillus niger, and catalase from bovine liver were bought from Sigma-Aldrich. The prostate cancer LNCaP cells and healthy RWPE-1 cells were obtained from ATCC. µ-Slide 8 well glass bottom chambered coverslips (#1.5H) were purchased from Ibidi. 5-Fluorouracil (≥98%) and doxorubicin hydrochloride (98-102%) were bought from Sigma-Aldrich while gemcitabine hydrochloride (98%) was purchased from Thermo Scientific. RPMI 1640 medium, keratinocyte-SFM serum free medium, supplements for keratinocyte-SFM, fetal bovine serum, penicillin-streptomycin, and trypsin-EDTA were obtained from Gibco. PrestoBlue cell viability reagent was bought from Thermo Fischer Scientific and 3-(4,5-dimethylthiazol-2-yl)-2,5-diphenyltetrazolium bromide (MTT) was purchased from Sigma-Aldrich.

Instruments. A JASCO V-650 UV-VIS Spectrophotometer was used to measure UV-visible absorption spectra of different samples including nanoparticles. The fluorescence spectra of the samples were recorded using FLS920 Fluorescence Spectrometer (Edinburgh Instruments) at room temperature. The hydrodynamic sizes and zeta potentials of nanoparticles were measured using Malvern Zetasizer Nano series Nano-ZS. Attenuated total reflectance Fourier transformed infrared (ATR-FTIR) spectra of samples were measured using a Perkin Elmer Spectrum Two FTIR spectrophotometer equipped with the diamond as an ATR crystal. ^{1}H NMR spectrum of Fmoc-Silane in $CDCl_3$ was recorded using Bruker Advance 200 MHz spectrophotometer. Solid-state ^{13}C and ^{29}Si NMR spectra of nanoPMOs were acquired on a 300 MHz Varian VNMRS300 spectrometer ("Wide Bore" magnet at 7.05 Tesla) using a Varian T3 MAS (Magic Angle Spinning) probe, with 3.2 mm ZrO_2 rotors. The transmission electron microscope (TEM) images of nanoparticles placed on the formvar/carbon-coated copper grid were acquired by TEM (JEOL 1400 Plus) operated at 120 kV. The energy dispersive X-ray spectrum (EDS) and elemental mapping images of nanoparticles were acquired by TEM (JEOL 2200FS) operated at 200 kV. For elemental analysis by TEM, holey carbon-supported copper grids were used. Nitrogen adsorption-desorption isotherms of nanoparticles were recorded at 77K on a Micromeritics TriStar 3000 analyzer to calculate their surface area, pore volume, and pore size. All nanoparticles were degassed under a high vacuum at 80 ºC for 12 h before measurement. dSTORM images were acquired using a Nikon N-STORM super-resolution microscope

configured for TIRF imaging and equipped with a perfect focus system. During dSTORM imaging, Cy3 dye-labeled nanoparticles were excited by 561 nm laser (80 mW) while Cy5 dye-labeled antibodies were excited by 647 nm laser (160 mW) with an adjusted TIRF angle to maximize the signal-to-noise ratio. There was no UV activation. An oil immersion Nikon 100X objective, 1.49 NA, was used to collect fluorescence signals, which were processed through a quad-band pass dichroic filter (97335 Nikon) and then images were recorded using a Hamamatsu ORCA Flash 4.0 camera with pixels of 160 nm and a region of interest of 256 by 256 pixels.

Synthesis of cyanine 3 dye conjugated (3-aminopropyl)triethoxysilane (Cy3-APTES). Using more convenient succinimidyl ester chemistry, the Cy3 dye molecule was coupled with the silane molecule. Briefly, 10 µmol cyanine 3 NHS ester (6.415 mg) was dissolved in 700 µL anhydrous dimethylformamide (DMF). Next, 10 µmol (3-aminopropyl)triethoxysilane (2.34 µL) in 25 µL anhydrous DMF and 15 µmol triethylamine (2.1 µL) in 25 µL anhydrous DMF were added to the dye solution, respectively. The reaction mixture was stirred overnight at room temperature in an inert atmosphere and under a dark condition. Finally, the solution of Cy3-APTES was stored at 2-8 ºC and directly used to synthesize fluorescent nanoPMOs.

Synthesis of Cy3 labeled periodic mesoporous organosilica nanoparticles (nanoPMOs). Several fluorescent and biodegradable periodic mesoporous organosilica nanoparticles labeled with cyanine 3 dye were synthesized.[48] Briefly, in a 250 mL three neck round bottom flask, 686 µmol cetyltrimethylammonium bromide (250 mg) was dissolved in 120 mL distilled water and then 875 µL aqueous solution of NaOH (2 M) was added. The resulting solution was heated at 80 ºC for 50 min under the stirring condition at 1000 rpm. After that, the mixture of varied amounts of different silane molecules such as 1,4-bis(triethoxysilyl)benzene (BTEB), 1,2-bis(triethoxysilyl)ethylene (BTEE), bis(3-triethoxysilylpropyl)disulfide (BTEPDS), bis(3-triethoxysilylpropyl)tetrasulfide (BTEPTS), and Cy3-APTES were added to the reaction solution dropwise (Table S1). After continuing the reaction at 80 °C for 2 h, the solution was cooled to room temperature. In the following step, the nanoparticles were collected via centrifugation at 20000 rpm for 10 min. Most importantly, cetyltrimethylammonium bromide (CTAB) was removed from nanoparticles using an ethanolic solution of NH_4NO_3 (6 g/L) via 30 min sonication at 50 °C and centrifugation at 20000 rpm for 10 min. Further, the nanoparticles were washed with ethanol, water, and ethanol, respectively. Each wash consisted of sonicating the nanoparticle solution for 10 min at room temperature and centrifuging it under

the same conditions. Finally, the purified fluorescent nanoPMOs were dispersed in ethanol and were stored at 2-8 ºC in a dark environment.

Synthesis of Fmoc-Silane. The coupling between 9-fluorenylmethyl carbazate and 3-(triethoxysilyl)propyl isocyanate in order to synthesize Fmoc-Silane was successfully carried out via our method as published earlier with minor modification.[52] Briefly, 7.87 mmol 9-fluorenylmethyl carbazate (2 g) was placed into a 250 mL two-neck round bottom flask and dried under vacuum for 30 min at room temperature. Next, 9-fluorenylmethyl carbazate was suspended in 50 mL absolute ethanol and degassed the suspension with argon gas for 30 min. The degassed 7.87 mmol 3-(triethoxysilyl)propyl isocyanate (1.947 mL) was injected into the reaction medium under a stirring condition and an inert atmosphere. The reaction was continued for 4 h at room temperature until the suspension completely disappeared. After that, the solvent was completely removed using a rotary evaporator and the obtained solid residue was dissolved in 8 mL dichloromethane. Adding excess pentane precipitated the desired product, which was then filtered. In the next step, the solid product was washed three times with pentane before being dried under vacuum at room temperature. The pure Fmoc-Silane was stored at room temperature under a vacuum and inert atmosphere. ^{1}H NMR (200 MHz, $CDCl_3$) δ (ppm): 0.66 (t, 2H), 1.24 (t, 9H), 1.59-1.70 (m, 2H), 3.28 (t, 2H), 3.79 (q, 6H), 4.22 (t, 1H), 4.52 (d, 2H), 6.67 (s, 1H), 7.34-7.48 (m, 4H), 7.61 (d, 2H), 7.79 (d, 2H).

Synthesis of semicarbazide functionalized nanoPMOs. The nanoPMOs were functionalized with semicarbazide groups using the following protocol.[52] In brief, 60 mg nanoPMOs dispersed in 3 mL ethanol (96%) were mixed with 10 µL triethylamine followed by a 2 mL ethanol solution containing 200 mg Fmoc-Silane. The reaction mixture was stirred at 80 °C for 18 h in the dark. After that, 10 µL piperidine was added for Fmoc deprotection and the reaction was further continued for 30 min under identical conditions. The nanoparticles were washed four times with ethanol and then with distilled water. The nanoparticles was collected via centrifugation at 20000 rpm for 10 min. Finally, purified semicarbazide functionalized nanoPMOs were dispersed in Milli-Q water and stored at 2-8 °C.

Synthesis of carboxylic acid functionalized nanoPMOs. The nanoPMOs were functionalized with carboxylic acid via the following two steps.[54] In the first step, 60 mg nanoPMOs were mixed with 100 µL (3-aminopropyl)triethoxysilane in 5 mL ethanol (96%), followed by 18 h of stirring at 80 °C in the dark. The (3-aminopropyl)triethoxysilane grafted nanoparticles were then separated by centrifugation at 20000 rpm for 10 min. The nanoparticles were washed with

ethanol three times and collected via centrifugation under the same conditions. The nanoPMOs functionalized with amine groups were completely dried at room temperature under a vacuum. Nanoparticles were dispersed in 4 mL of anhydrous DMF and a solution of succinic anhydride (200 mg) in anhydrous DMF (2 mL) was added to the nanoparticle's solution in the next step. The reaction mixture was stirred under dark conditions at room temperature overnight. The carboxylic acid-functionalized nanoparticles were collected and then washed three times with distilled water in order to purify them. A similar centrifugation technique was used to collect the nanoparticle pellet. Finally, purified nanoPMOs functionalized with carboxylic acid were dispersed in Milli-Q water and then stored at 2-8 °C.

Fluorescamine assay. In order to determine the presence of primary amine groups on the nanoparticle's surface, the fluorescamine assay was performed by a previously published protocol.[53] In brief, 1.5 mL aqueous solution of nanoparticles (1 mg/mL) was mixed with a freshly prepared fluorescamine solution (1.5 mL) in ethanol at a concentration of 1 mg/mL. Next, 200 µL 10 mM borate buffer (pH 9) was added to the mixture, which was allowed to stand at room temperature under a dark condition for one hour. The fluorescence of solutions was measured at an excitation wavelength of 390 nm.

Oxidation and Cy5 dye labeling of the antibody. The oxidation of carbohydrate residues present on the anti-M6PR antibody was performed by following the protocol published previously.[52] Briefly, 50 µL antibody solution (1 mg/mL) was diluted to 1 mL solution with phosphate buffer (10 mM, pH 7.4). Next, 25 µL aqueous solution of sodium periodate (0.1 M) was added to the antibody solution. The mixture was incubated in the dark at room temperature for 1 h. The oxidized antibody was then purified by a PD-10 disposable desalting column and the amount of collected antibody was determined via measuring the absorbance at 280 nm using a Nanodrop ND-1000 spectrophotometer.

For conjugation of cyanine 5 (Cy5) dye with primary amine groups of oxidized antibody, the phosphate buffered solution of oxidized antibody (pH 7.4) was mixed with cyanine 5 NHS ester solution (dissolved in DMSO) at an approximate molar ratio of 1:5. The reaction was continued for 6 h at room temperature in a dark environment. Next, the Cy5 dye labeled antibody was separated from free dye molecules using a PD-10 disposable desalting column. The approximate concentration of antibody and Cy5 dye were calculated via measuring the absorbance at 280 nm and 646 nm, respectively using a Nanodrop ND-1000 spectrophotometer.

Calculation of degree of Cy5 dye labeling. The approximate number of Cy5 dye labeled per antibody was calculated using UV-visible absorption spectroscopy. At first, the molar excitation coefficient of the anti-M6PR antibody was measured from the following formula of Beer-Lambert law.

$$A = \varepsilon cl$$

Where A is the absorbance of the antibody at 280 nm, ε is the molar excitation coefficient to be determined, c is the molar concentration of the antibody, and l is the optical path length (typical value is 1 cm).

The calculated value of ε for the anti-M6PR antibody was 399282 $M^{-1}cm^{-1}$.

Similarly, the molarity of Cy5 dye present on Cy5 dye labeled anti-M6PR antibody was calculated and the value was 4.8 X 10^{-8} M.

In contrast, the molarity of the antibody labeled with Cy5 dye was calculated by the following equation.

$$\text{Molarity of antibody} = \frac{A_{280} - (A_{646} \text{ X CF})}{\varepsilon}$$

Where A_{280} is the absorbance of the antibody at 280 nm, A_{646} is the absorbance of Cy5 dye at 646 nm, and CF is the correction factor for Cy5 dye (the value of 0.05 was considered).

The calculated value was 4.86 X 10^{-8} M.

$$\text{The number of Cy5 dye per antibody} = \frac{\text{molarity of Cy5 dye}}{\text{molarity of antibody}}$$

Therefore, the calculated number of Cy5 dye per antibody was 0.99.

Antibody conjugation. The oriented conjugation of anti-M6PR antibody with nanoPMOs was performed via the most common condensation reaction between semicarbazide groups of nanoparticles and aldehyde groups present on the oxidized antibody.[52,55] In brief, approximate 20 or 4 pmol Cy5 labeled anti-M6PR antibody in phosphate buffer solution (pH 7.4, 10 mM) was mixed with semicarbazide functionalized nanoPMOs (0.5 mg) and then the mixture was stirred for 6 h at room temperature in the dark. Next, antibody conjugated nanoparticles were collected via centrifugation at 13000 rpm for 10 min and subsequently washed several times with 10 mM phosphate buffer pH 7.4. The purified antibody conjugated nanoparticles were finally dispersed in Milli-Q water (500 µL) and stored at 2-8 ºC.

For random conjugation of anti-M6PR antibody with nanoparticles, two steps carbodiimide-based coupling reaction was utilized.[55] At first, 0.5 mg carboxylic acid functionalized nanoPMO nanorods were dispersed in 10 mM MES buffer (pH 5.5) and then 5 nmol 1-ethyl-3-(3-dimethylaminopropyl)carbodiimide hydrochloride and 100 nmol N-hydroxysuccinimide were added to the nanoparticle's solution. The mixture was stirred for 45 min at room temperature to activate the carboxylic groups of nanoparticles. The nanoparticles with activated carboxyl groups were collected via centrifugation at 13000 rpm for 12 min. Subsequently, the nanoparticles were dispersed in 10 mM phosphate buffered solution (pH 7.4) containing approximate 20 pmol Cy5 labeled anti-M6PR antibody and incubated in the dark for 6 h under a stirring condition for the reaction between primary amine groups of antibody and activated carboxyl groups of nanoparticles. Next, antibody conjugated nanoparticles were washed several times with phosphate buffer (10 mM, pH 7.4) and dispersed in 500 µL Milli-Q water. Finally, the aqueous solution of nanoparticles conjugated with antibody was stored at 2-8 ºC.

Monitoring the degradation of nanoPMOs by TEM. The glutathione-responsive degradation of various functionalized nanoPMOs was evaluated in phosphate buffered solution of 10 µM and 10 mM reduced glutathione. Briefly, 0.5 mg semicarbazide functionalized nanoparticles or carboxylic acid functionalized nanoparticles was dispersed in 10 mM phosphate buffer pH 7.4 (5 mL) with different concentrations of glutathione (10 µM and 10 mM). The resulting nanoparticle solution was stirred at room temperature under an ambient atmosphere. At different incubation time points (up to 7 days), aliquots (200 µL) were taken and diluted with one mL Milli-Q water. The diluted solution was used to visualize the nanoparticle's degradation by transmission electron microscope (TEM).

dSTORM imaging of nanoPMOs and antibody conjugated nanoPMOs. For dSTORM imaging of nanoPMOs and antibody conjugated nanoPMOs, the flow chambers with an approximate volume of 30-40 µL were initially constructed by attaching a coverslip on a glass microscopy slide using double-sided scotch tape.[45,51] To immobilize the nanoparticles on the coverslip, 40 µL phosphate buffered solution (10 mM, pH 7.4) of nanoparticles at a concentration of 100 µg/mL was placed into the chamber and then incubated for 10 min. Next, the unbound nanoparticles were washed with dSTORM buffer solution consisting of 5% (w/v) glucose, 10 mM cysteamine, glucose oxidase (0.56 mg/mL) and catalase (34 µg/mL) in 10 mM PBS solution (pH 7.4) three times. Subsequently, the flow chambers were filled with dSTORM buffer solution and sealed with transparent nail polish. The nanoparticles labeled with Cy3 dye

were imaged by acquiring 30000 frames at 10 ms exposure time under 561 nm laser excitation with 100% laser power. In addition to this, 20000 frames of fluorescence signal from Cy5 dye labeled antibody was consequently acquired using 647 nm laser at 75% laser power excitation for antibody conjugated nanoparticles.

Evaluation of nanoPMOs degradation by dSTORM. To evaluate the degradation of nanoPMOs by reduced glutathione, the semicarbazide functionalized nanoparticles or carboxylic acid functionalized nanoparticles (50 µg) was initially incubated in 500 µL phosphate buffered solution of glutathione (10 mM, pH 7.4) with different concentrations (10 µM and 10 mM) under stirring condition for different times. After different time points, the resulting nanoparticles solution (40 µL) at a concentration of 100 µg/mL was placed into the flow chamber and then allowed to stand for 10 min in order to immobilize them on coverslips. Next, dSTORM buffer solution was used to wash and then fill the flow chambers, and subsequently, the chambers were sealed with transparent nail polish. For dSTORM imaging, the fluorescence signals of Cy3 dye were collected in 30000 frames at 10 ms exposure time under 561 nm laser excitation at 100% laser power. In contrast, a 647 nm laser at 75% laser power was used to excite Cy5 dye and their fluorescence signals were similarly recorded in 20000 frames.

Loading of anticancer drugs. The anticancer drug molecules were loaded into the porous structure of nanoPMOs by mixing nanoparticles (1 mg) with the drug (350 µg) in 500 µL phosphate buffer (10 mM, pH 7.4) or acetate buffer (10 mM, pH 5). The mixture was stirred at room temperature overnight under a dark condition. To remove the free drug, drug-loaded nanoPMOs were collected via centrifugation (13000 rpm, 12 min) followed by washing four times with Milli-Q water. The amount of unloaded drug was quantified by measuring the absorbance of the supernatant. Finally, the drug-loaded nanoparticles were dispersed in Milli-Q water and stored at 2-8 °C. The loading content (LC) of drug into nanoparticles was calculated using the equation: loading content (%) = (weight of drug loaded into nanoparticles/weight of nanoparticles) X 100. In contrast, drug encapsulation efficiency (EE) of nanoparticles was determined using an equation of encapsulation efficiency (%) = (weight of drug loaded/ weight of drug used) X 100.

Responsive drug release. The glutathione responsive drug release study was carried out in 10 mM phosphate buffer (pH 7.4) or acetate buffer solution (pH 5) containing 10 µM and 10 mM reduced glutathione. Typically, 50 µL doxorubicin loaded nanoPMOs (1 mg/mL) were mixed with glutathione solution (450 µL) and then stirred at room temperature for different times. The

released doxorubicin was collected via centrifugation at 13000 rpm for 20 min. The amount of released doxorubicin at different time points was determined via measuring the absorbance of the supernatant at 490 nm. The quantification of drug release was performed by the formula: drug release (%) = (amount of released drug/amount of loaded drug) X 100.

Cell culture. Human prostate cancer LNCaP cells were cultured in RPMI-1640 medium supplemented with 10% fetal bovine serum and 1% penicillin-streptomycin and human rhabdomyosarcoma Rh30 cells were grown in Dulbecco's Modified Eagle Medium supplemented with 10% fetal bovine serum and 1% penicillin-streptomycin. In contrast, human healthy prostate cell line RWPE-1 was cultivated in keratinocyte-SFM serum free medium supplemented with human recombinant epidermal growth factor and bovine pituitary extract and also 1% penicillin-streptomycin. Both cells were grown in a humidified atmosphere at 37 ºC with 5% CO_2. After 70-80% cell confluency, trypsin-EDTA was used to detach the cells for subculture.

Cell viability assay. *In vitro* cytotoxicity of nanoparticles was measured by the PrestoBlue cell viability assay.[58] Briefly, LNCaP and RWPE-1 cells (~10000 cells/well) were seeded into 96-well flat bottom tissue culture plate using a 100 µL cell culture medium and then incubated for 24 h at 37 ºC with 5% CO_2. Afterward, the cells were treated with nanoparticles at different concentrations in the range of 2.5-100 µg/mL for 24 h. The cells without any treatment were considered as a negative control. Next day, the culture medium containing free nanoparticles was removed from the wells. After that, 100 µL PrestoBlue reagent (10%, v/v) in the fresh culture medium was added to each well followed by incubation for 2 h at 37 ºC. The absorbance (A) of the resulting solutions was measured at 570 and 600 nm using a Tecan Infinite M200 PRO multimode microplate reader. Each nanoparticle at the same concentration was tested in triplicate. The cell viability was calculated by the following equation.

$$\text{Cell viability (\%)} = \frac{(A_{570} - A_{600})_{\text{sample}}}{(A_{570} - A_{600})_{\text{control}}} \text{ X } 100$$

The results were presented as a mean ± standard deviation.

Flow cytometry. The interaction of various nanoPMOs functionalized with and without antibody with prostate cancer LNCaP cells and human rhabdomyosarcoma Rh30 cells was quantitatively evaluated using a flow cytometry analysis.[33] The cells were seeded in a 12-well plate at a density of 10^5 cells/well and left to grow for 48 h at 37 ºC with 5% CO_2. After, the

cells were treated with different nanoparticles at a final concentration of 50 µg/mL and incubated for 6 h. After being washed twice with PBS solution, cells were trypsinized, then collected in a culture medium, and centrifuged for 5 min at 1300 rpm. Next, the cell pellets were suspended in 200 µL PBS solution containing $MgCl_2$ and $CaCl_2$ and kept on ice until the measurement. The flow cytometry was performed using a NovoCyte flow cytometer and the data were analyzed by NovoExpress software (ACEA Biosciences, Inc.). The evaluation of the nanoparticle internalization was carried out in 20,000 events. The experiment was repeated twice.

dSTORM imaging of cells. Both prostate cancer LNCaP cells and healthy RWPE-1 cells were seeded into µ-slide 8 well glass bottom chambered coverslip at a density of 10000 cells/well with 300 µL cell culture medium and then allowed to grow at a condition of 37 ºC with 5% CO_2.[45,51] Next, the cells were treated with different types of nanoparticles at a concentration of 6 µg/mL and subsequently incubated for different times (1-6 h). After incubation, the cells were washed with PBS solution (10 mM, pH 7.4) three times to remove free nanoparticles mainly. The washed cells were then fixed *via* incubating the cells with 4% paraformaldehyde solution at room temperature for 15 min. After three washes with PBS solution, the fixed cells were stored with PBS solution at 2-8 ºC. For dSTORM imaging of cells, PBS solution was replaced by dSTORM buffer solution (200 µL). The fluorescence signal of Cy3 dye labeled nanoparticles was collected in 30000 frames at 10 ms exposure time under excitation of 561 nm laser with 100% laser power. Subsequently, 20000 frames of fluorescence signal from Cy5 dye attached with antibody was acquired using 647 nm laser at 75% laser power excitation.

Analysis of dSTORM data. Nikon NIS elements software was used to analyze dSTORM images. A Gaussian fitting of blinking dyes with a minimum intensity height threshold of 200 for the 561 channel of Cy3 dye-labeled nanoparticles and 180 for the 647 channel of Cy5 labeled antibody detected dSTORM localizations. In order to eliminate the nonblinking behavior in the first instance of the sample illumination, the analysis started with frame number 800 for nanoparticle imaging and 100 for antibody imaging. To analyze the dSTORM images to quantify the size of nanoparticles and the number of localizations, we imported the dSTORM localization list and ran it through a custom MATLAB script as mentioned in our previous studies.[45,51] A mean shift clustering algorithm was applied to cluster the 561 localizations produced from Cy3 dye-labeled nanoPMOs and also quantify the localization number generated in 647 channels corresponding to antibodies labeled with Cy5 dye.

In vitro anticancer activity. The MTT assay was performed in order to access the cytotoxicity of free doxorubicin (DOX), nanoPMOs, and DOX loaded nanoPMOs toward prostate cancer cells.[33] For the cytotoxicity study, we seeded 10^4 LNCaP cells *per* well and incubated them for 24 h in 96-well plates. After that, the cells were treated with DOX, nanoparticles, and DOX loaded nanoparticles at different levels of drug concentration (0-750 ng/mL), or nanoparticle concentration (0-2.5 µg/mL) and incubated for a variety of times (1, 2, and 3 days). Cells treated with the vehicle were considered as control. After washing the cells with PBS solution, MTT solution was added to the cells at a final concentration of 0.5 mg/mL, and the cells were incubated for 4 h at 37 ºC. The produced purple formazan crystals were dissolved in a mixture of ethanol and DMSO (1:1, v/v %). The absorbance (A) of the resulting solutions was measured using Multiskan Sky Microplate Spectrophotometer (Thermo Fisher Scientific) at 540 nm. Finally, the percentage (%) of viable cells was calculated from the following equation: cell viability = $(A_{sample}/A_{control})$ X 100. A dose response curve of cell viability versus the log of concentration was used to determine the lethal concentration (LC_{50}) value.

Table S1. Preparation of BTEB-based (BPMO) or BTEE-based (EPMO) fluorescent nanoPMOs with or without disulfide or tetrasulfide bridges.

nanoPMOs	Amount of BTEB (mmol)	Amount of BTEE (mmol)	Amount of BTEPDS (mmol)	Amount of BTEPTS (mmol)	Amount of Cy3-APTES (nmol)
BPMO	2.292	---	---	---	9.16
BPMO (90/10)	2.063	---	0.229	---	9.16
BPMO TS (90/10)	2.063	---	---	0.229	9.16
EPMO	---	2.292	---	---	9.16
EPMO (90/10)	---	2.063	0.229	---	9.16
EPMO (75/25)	---	1.719	0.573	---	9.16
EPMO (60/40)	---	1.375	0.917	---	9.16

Table S2. Various physicochemical properties of fluorescent and biodegradable nanoPMOs used in this study.

nanoPMOs	Shape	Size (nm)[¶] & aspect ratio	Hydrodynamic size (nm) & PDI	Zeta potential (mV)	Optical size[#] (nm)	Surface area (m^2/g)	Pore size (nm)	Pore volume (cm^3/g)
BPMO	nanosphere	197, ~1	291, 0.184	-33.1	108	1377	2.9	0.99
BPMO (90/10)	nanosphere	181, ~1	274, 0.119	-31.7	107	1465	2.6	1.19
BPMO TS (90/10)	nanosphere	165, ~1	253, 0.115	-34.2	86	1263	2.8	0.94
EPMO	nanorod	379 x 146, 2.54	365, 0.193	-34.1	149	1304	2.9	1.47
EPMO (90/10)	nanorod	329 x 136, 2.39	334, 0.255	-31.4	143	1567	2.7	1.09
EPMO (75/25)	nanorod	292 x 122, 2.37	293, 0.156	-33.6	152	1538	2.5	1.32
EPMO (60/40)	nanorod	195 x 107, 1.79	244, 0.245	-35.4	149	942	4.1	0.86

[¶] Average size of nanoparticles was measured from TEM images.
[#] Average optical size of nanoparticles was calculated from dSTORM analysis.

Table S3. Estimation of the quantity of silicon and sulfur elements present in various nanoPMOs nanorods by EDS analysis.

Sample	Atomic% of silicon	Atomic% of sulfur
EPMO	100	0
EPMO (90/10)	92	8
EPMO (75/25)	80.5	19.5
EPMO (60/40)	71.5	28.5

Table S4. The elemental composition of EPMO (60/40) nanorod measured by the energy dispersive X-ray spectroscopy (EDS) elemental analysis.

Element	Weight%	Atomic%
Carbon (C)	34.51	47.05
Oxygen (O)	34.61	35.43
Silicon (Si)	24.18	14.10
Sulfur (S)	6.70	3.42

Table S5. List of the abbreviations used for various surface modified nanoPMOs in this study.

Description of surface modified nanoPMOs	Abbreviation
Semicarbazide functionalized BPMO	BSC1
Semicarbazide functionalized BPMO (90/10)	BSC2
Semicarbazide functionalized BPMO TS (90/10)	BSC3
Semicarbazide functionalized EPMO	ESC1
Semicarbazide functionalized EPMO (90/10)	ESC2
Semicarbazide functionalized EPMO (75/25)	ESC3
Carboxylic acid functionalized EPMO (75/25)	ESA3
Semicarbazide functionalized EPMO (60/40)	ESC4
Carboxylic acid functionalized EPMO (60/40)	ESA4

Table S6. List of the abbreviations used for various antibody conjugated nanoPMOs in this study.

Surface modified nanoPMOs	Antibody conjugation approach	Density of antibody	Abbreviation
BSC1	oriented	high	BAB1H
BSC2	oriented	high	BAB2H
BSC3	oriented	high	BAB3H
ESC1	oriented	high	EAB1H
ESC2	oriented	high	EAB2H
ESC3	oriented	low	EAB3L
ESC3	oriented	high	EAB3H
ESA3	random	high	EBA3H*
ESC4	oriented	low	EAB4L
ESC4	oriented	high	EAB4H
ESA4	random	high	EBA4H*

Table S7. A summary of anticancer drug encapsulation efficiency (EE) and loading content (LC) of various functional nanoPMOs at physiological pH.

Functional nanoPMOs	Drug	EE (%)	LC (%)
BSC1	DOX	86.8%	30.4%
BSC2	DOX	89.7%	31.4%
BSC3	DOX	85.4%	29.9%
ESC1	DOX	86.5%	30.3%
ESC2	DOX	87.7%	30.7%
ESC3	DOX	94.2%	32.9%
ESA3	DOX	89.7%	31.4%
ESC4	5-FU	3%	0.9%
ESA4	5-FU	0.7%	0.2%
ESC4	GEM	7.6%	1.9%
ESA4	GEM	2.4%	0.6%
ESC4	DOX	86.8%	30.4%
ESA4	DOX	83.9%	29.3%
EAB4H	DOX	82.1%	28.7%

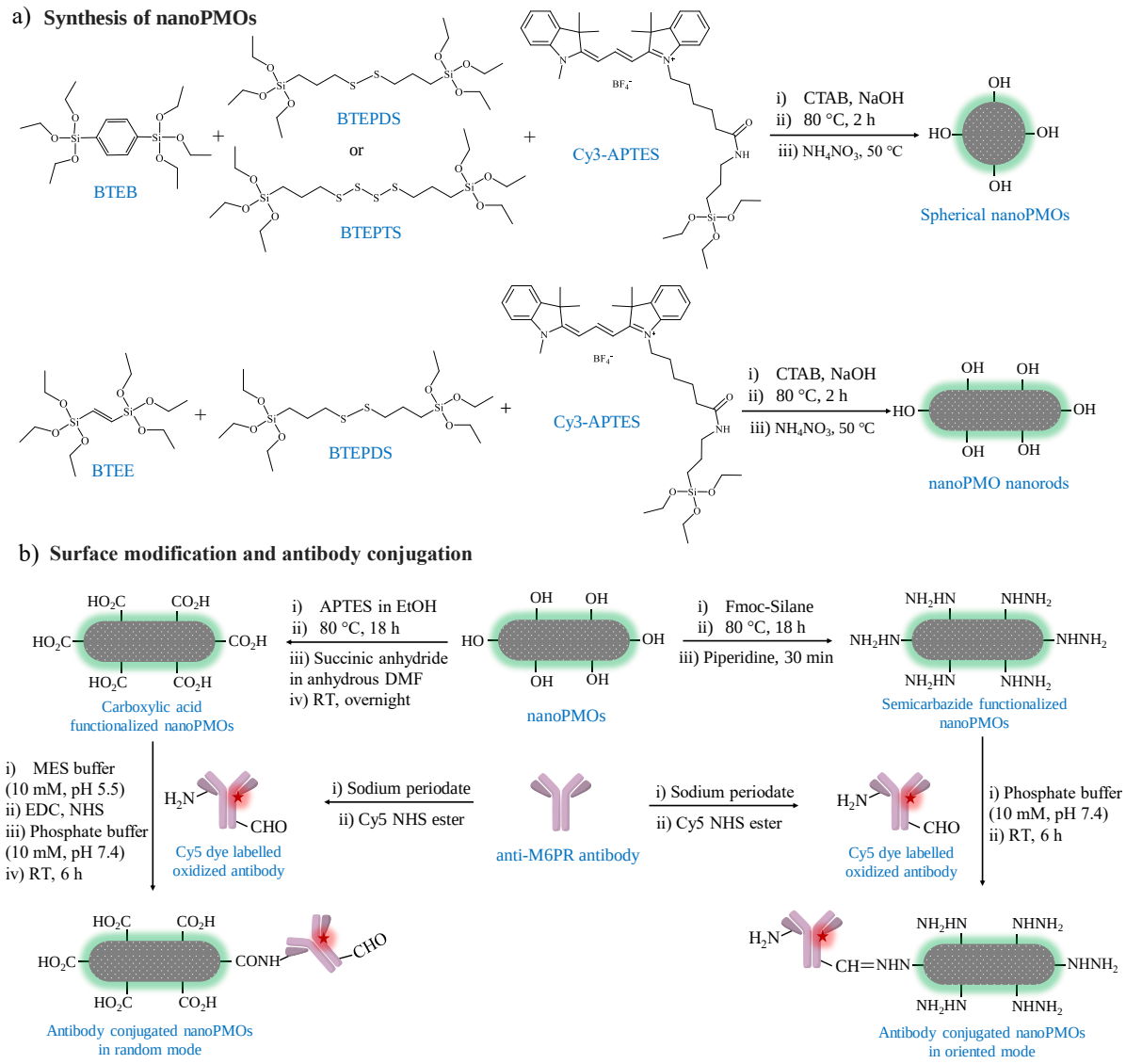

Scheme S1. Schematic illustration of the fabrication of antibody-conjugated nanoPMOs. a) Synthesis of fluorescent and biodegradable nanoPMOs with varied sizes, shapes, and compositions derived from different organosilane precursors using the sol-gel technique. b) The surface modification of nanoPMOs to produce nanoPMOs with different surface functional groups, which subsequently coupled with post-engineered fluorescent and oxidized anti-M6PR antibodies in oriented and random ways, resulting in a series of antibody-conjugated nanoPMOs.

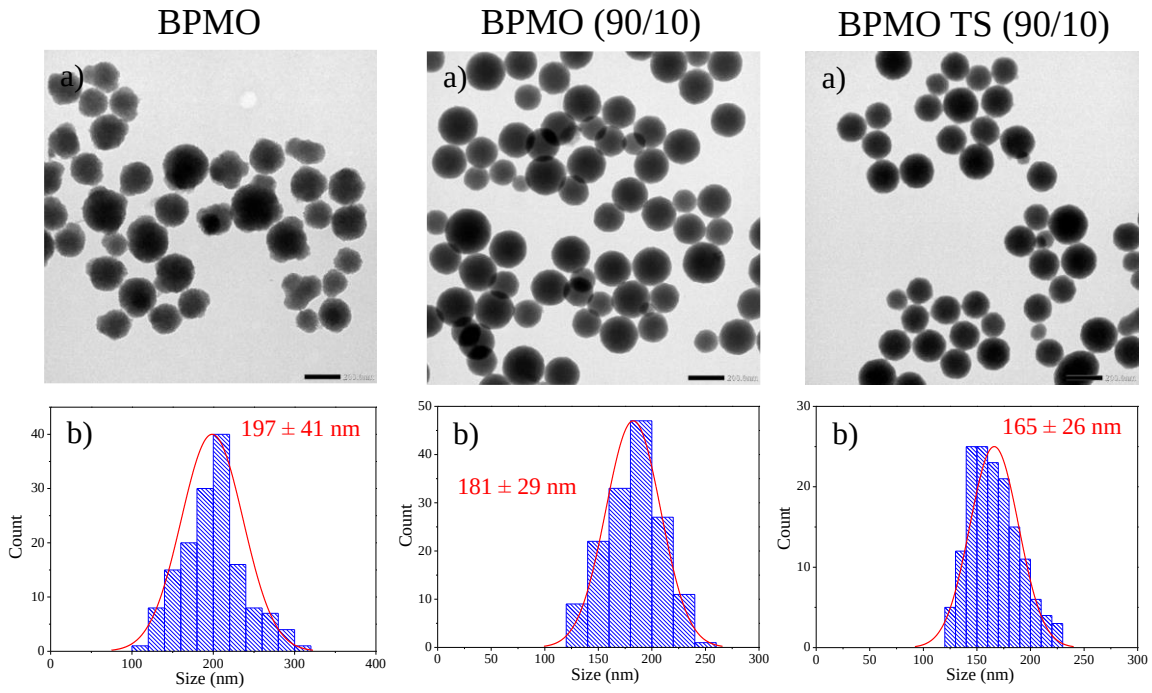

Figure S1. a) Representative low-resolution transmission electron microscope (TEM) images of three different spherical BTEB-based nanoPMOs. The scale bars of TEM images are 200 nm. b) The size distribution histogram of these nanospheres, measured from the TEM images. The insets present the calculated average diameter of nanoparticles.

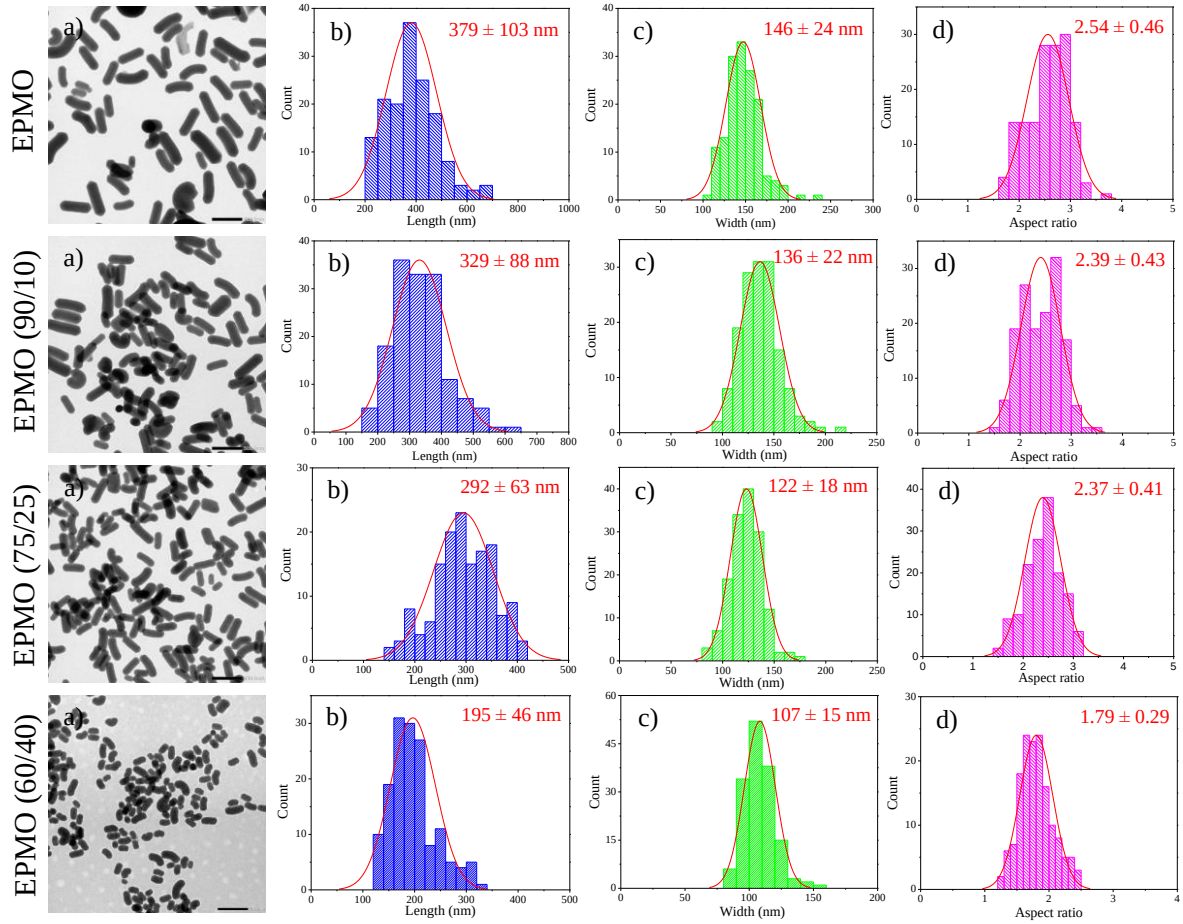

Figure S2. a) Representative low-resolution transmission electron microscope (TEM) images of four different BTEE-based nanoPMO nanorods. The scale bars of TEM images are 500 nm. b-d) The distribution histogram of their length, width, and aspect ratio, respectively measured from the TEM images. The insets show the calculated average value ± std. dev.

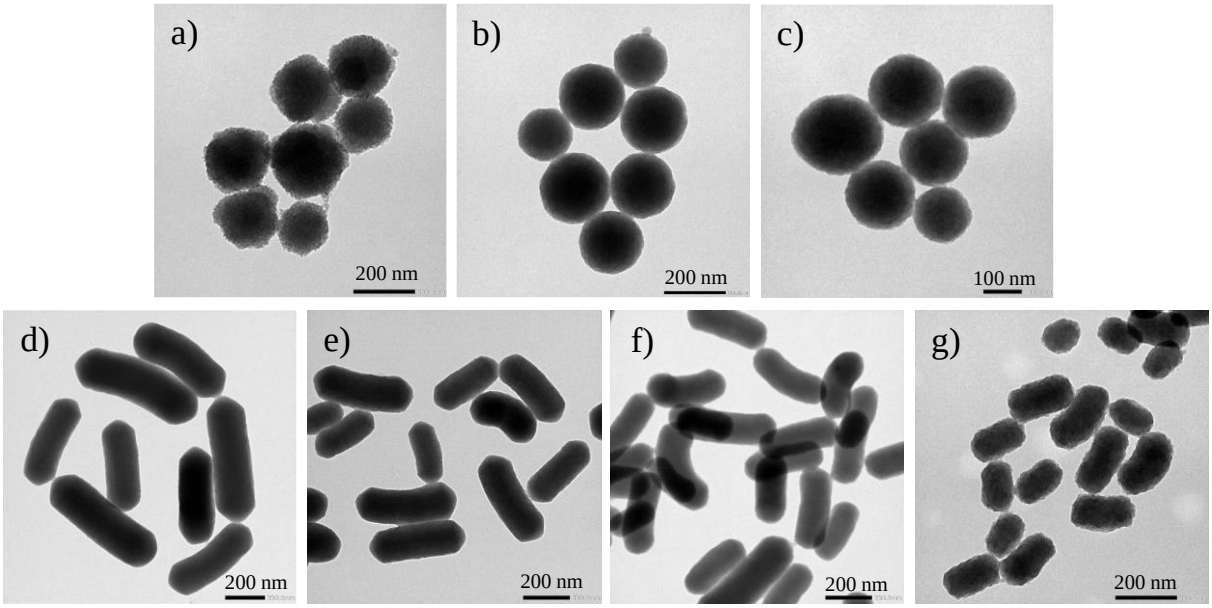

Figure S3. Representative transmission electron microscope (TEM) images at higher magnification of a) BPMO nanosphere, b) BPMO (90/10) nanosphere, c) BPMO TS (90/10) nanosphere, d) EPMO nanorod, e) EPMO (90/10) nanorod, f) EPMO (75/25) nanorod, and g) EPMO (60/40) nanorod.

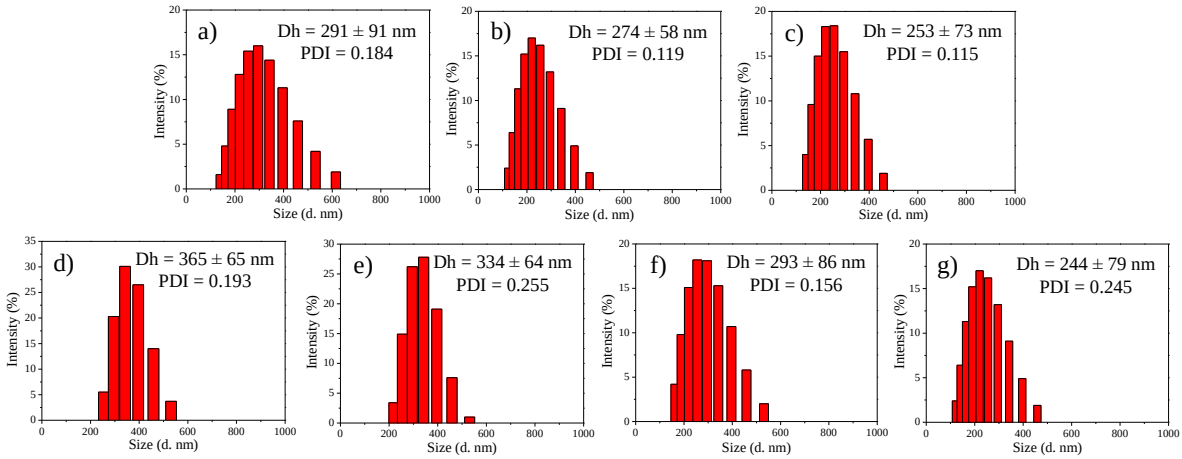

Figure S4. The hydrodynamic size distribution of various nanoparticles measured by dynamic light scattering method. a) BPMO nanosphere, b) BPMO (90/10) nanosphere, c) BPMO TS (90/10) nanosphere, d) EPMO nanorod, e) EPMO (90/10) nanorod, f) EPMO (75/25) nanorod, and g) EPMO (60/40) nanorod. The average hydrodynamic size (Dh), and polydispersity index (PDI) of nanoparticles are presented in the inset.

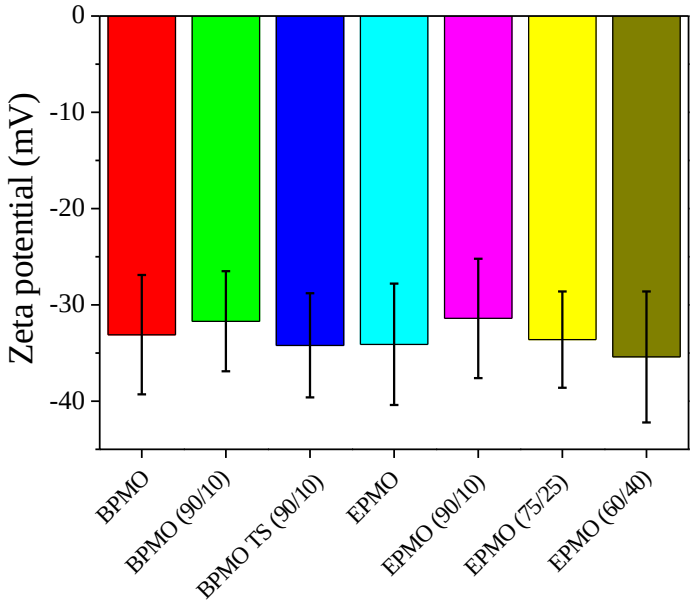

Figure S5. Zeta potentials of various nanoPMOs dispersed in distilled water which indicate the negative surface charge of all nanoPMOs.

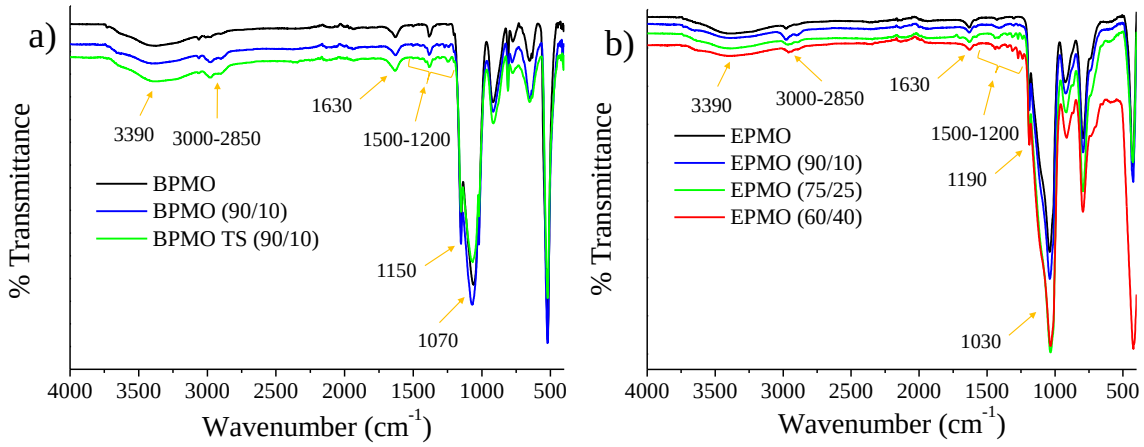

Figure S6. ATR-FTIR spectra of a) various nanoPMO nanospheres synthesized from 1,4-bis(triethoxysilyl)benzene and b) several nanoPMO nanorods synthesized from 1,2-bis(triethoxysilyl)ethylene. The characteristic peaks of organosilica precursor of nanospheres at 1630, 1150, and 1070 cm^{-1} correspond to the C=C, Si-C, and Si-O bonds, respectively. In contrast, nanorods show the characteristic peaks for the C=C, Si-C, and Si-O bonds at 1630, 1190, and 1030 cm^{-1}. Furthermore, the presence of silanol groups in both nanoPMOs is confirmed by the broad peak around 3390 cm^{-1}. The appearance of additional multiple peaks in the region of 3000-2850 cm^{-1} for C-H stretching and 1500-1200 cm^{-1} for C-H bending is attributed to the presence of the methylene groups of disulfide or tetrasulfide organosilane, indicating their successful co-hydrolysis/condensation.

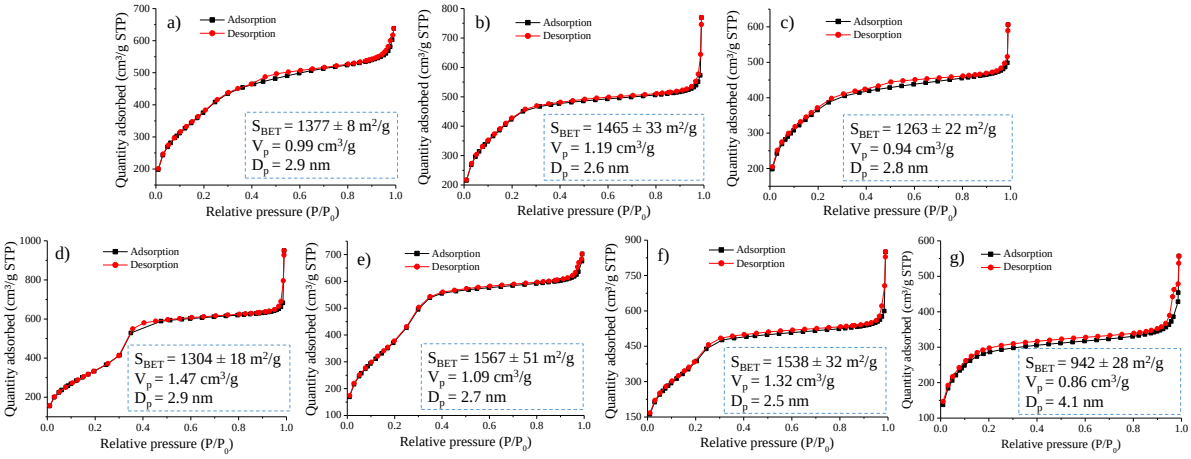

Figure S7. Nitrogen adsorption-desorption isotherms of a) BPMO nanosphere, b) BPMO (90/10) nanosphere, c) BPMO TS (90/10) nanosphere, d) EPMO nanorod, e) EPMO (90/10) nanorod, f) EPMO (75/25) nanorod, and g) EPMO (60/40) nanorod. The insets show the value of the surface area (S_{BET}), pore volume (V_p), and pore diameter (D_p) of the corresponding mesoporous nanoparticles.

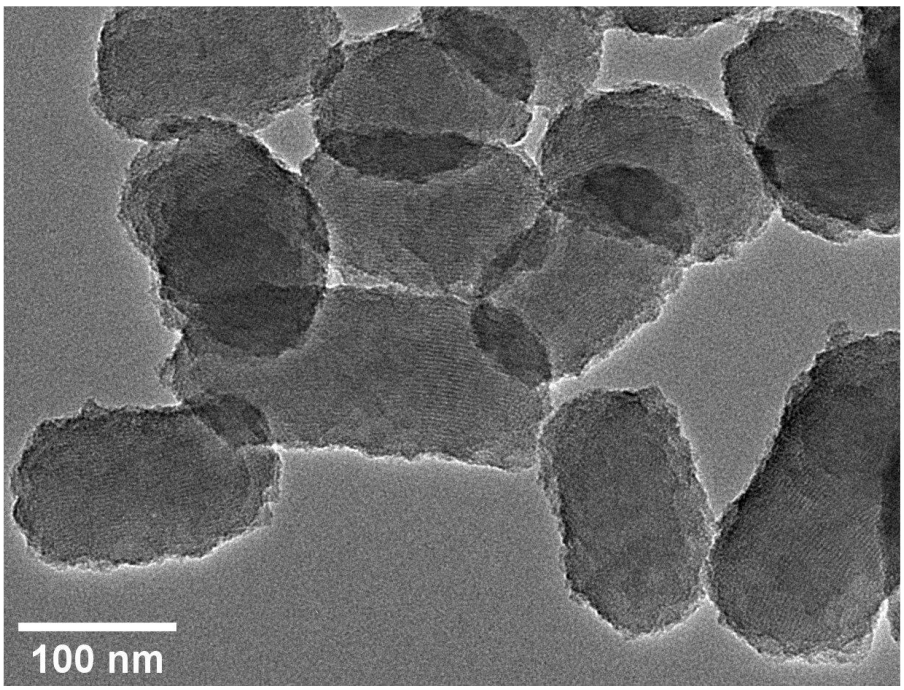

Figure S8. Representative TEM image of EPMO (60/40) nanorods, demonstrating the porous structure.

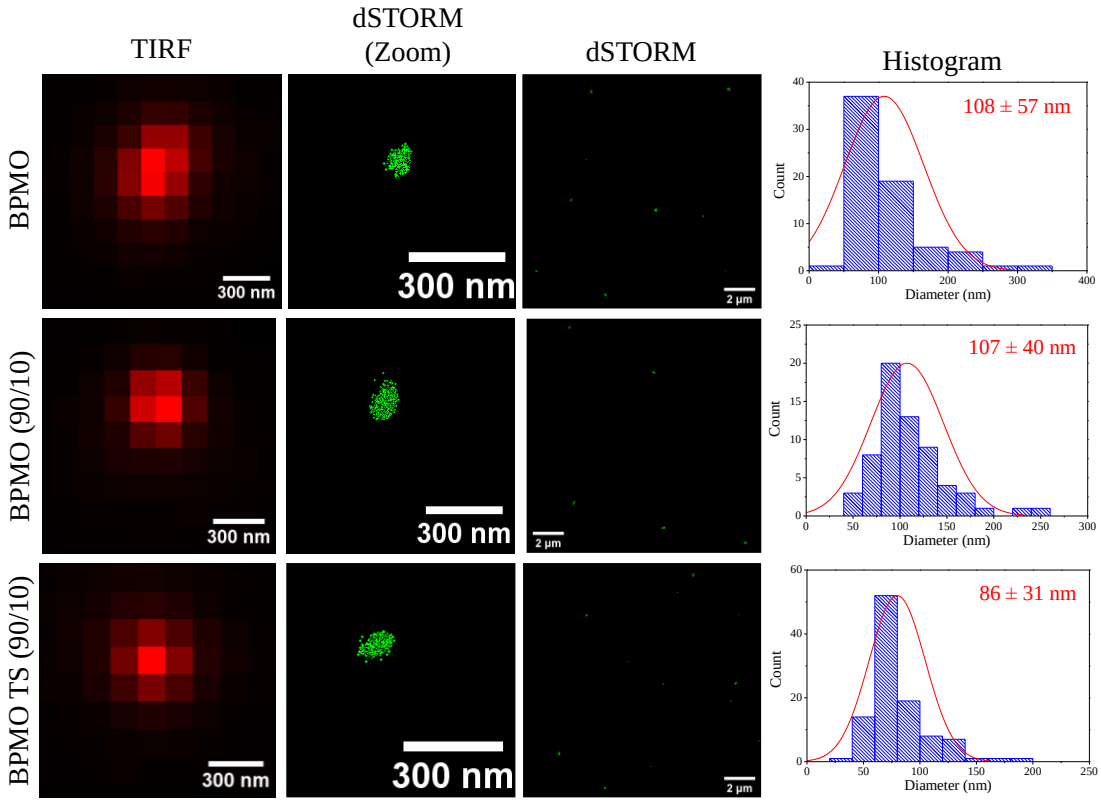

Figure S9. Total internal reflection fluorescence (TIRF) images of single BTEB-based nanoPMO nanospheres and their direct stochastic optical reconstruction microscopy (dSTORM) images in zoom mode are shown in the first and second columns, respectively. The third and fourth columns display the dSTORM images and the size distribution measured from the dSTORM of these nanoparticles, respectively. The average optical sizes are presented in the inset of their histogram.

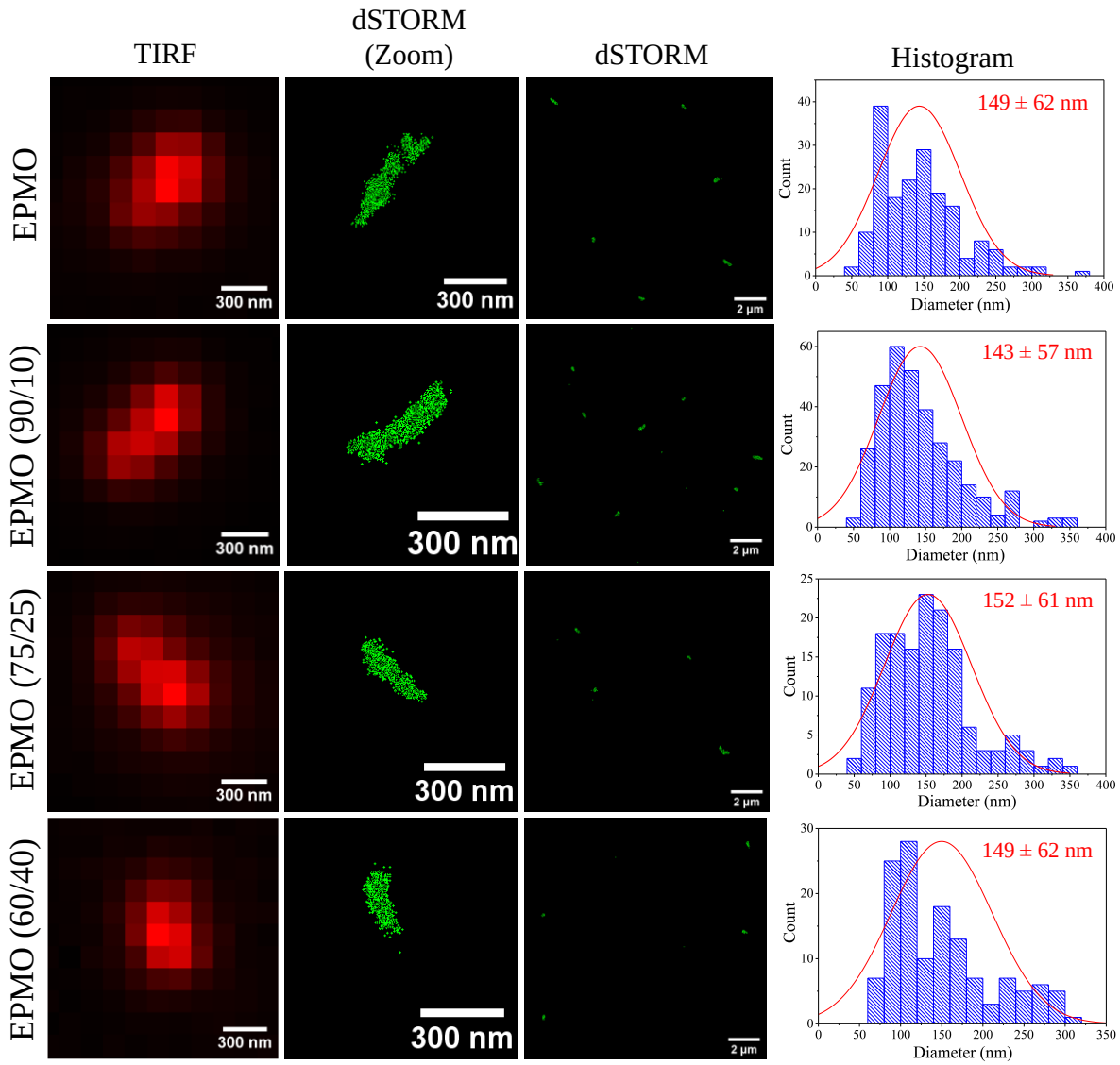

Figure S10. Total internal reflection fluorescence (TIRF) images of single BTEE-based nanoPMO nanorods and their direct stochastic optical reconstruction microscopy (dSTORM) images in zoom mode are shown in the first and second columns, respectively. The third and fourth columns display the dSTORM images and the size distribution measured from the dSTORM of these nanoparticles, respectively. The average optical sizes are presented in the inset of their histogram.

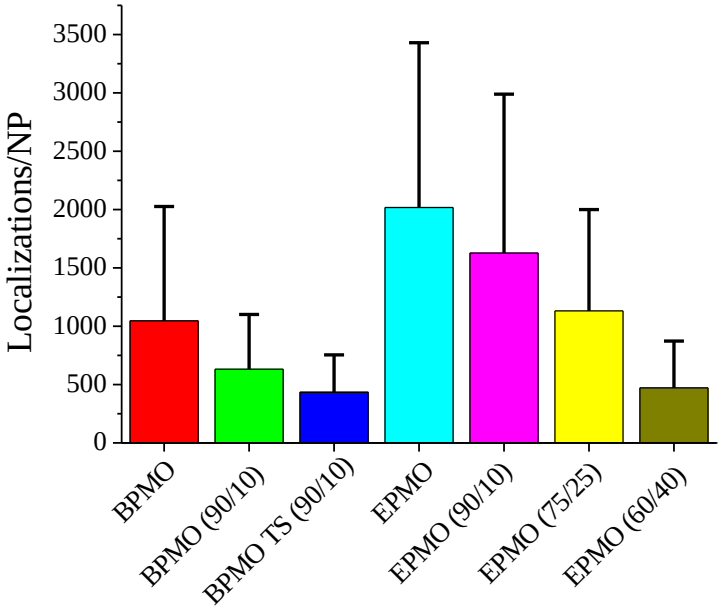

Figure S11. The number of localizations *per* nanoparticle produced from Cy3 dye blinking of different fluorescent nanoPMOs.

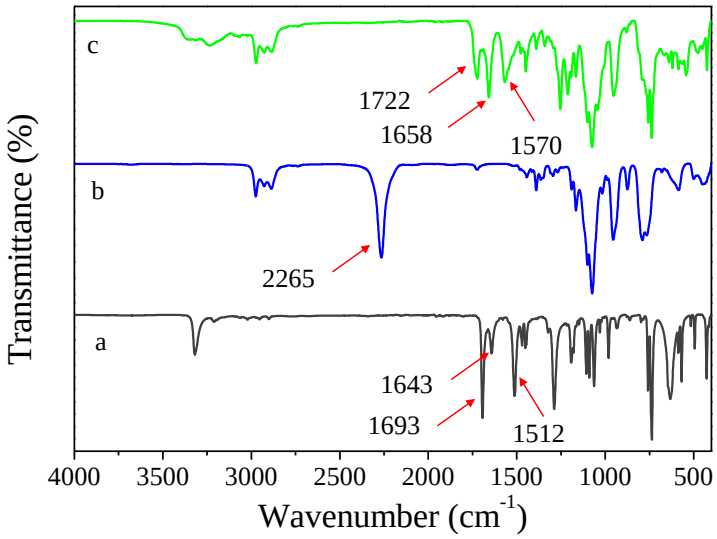

Figure S12. ATR-FTIR spectra of a) 9-fluorenylmethyl carbazate, b) 3-(triethoxysilyl)propyl isocyanate and c) Fmoc-Silane. The disappearance of the band at 2265 cm^{-1} corresponding to the isocyanate group and the shifting of C=O stretching for ester (i.e., from 1693 cm^{-1} to 1722 cm^{-1}) and amide groups (i.e., from 1643 cm^{-1} to 1658 cm^{-1}) and N-H bending vibration of amide groups from 1512 cm^{-1} to 1570 cm^{-1}, and also the enhancement of amide bands intensity at 1658 cm^{-1} indicates the successful formation of Fmoc-Silane.

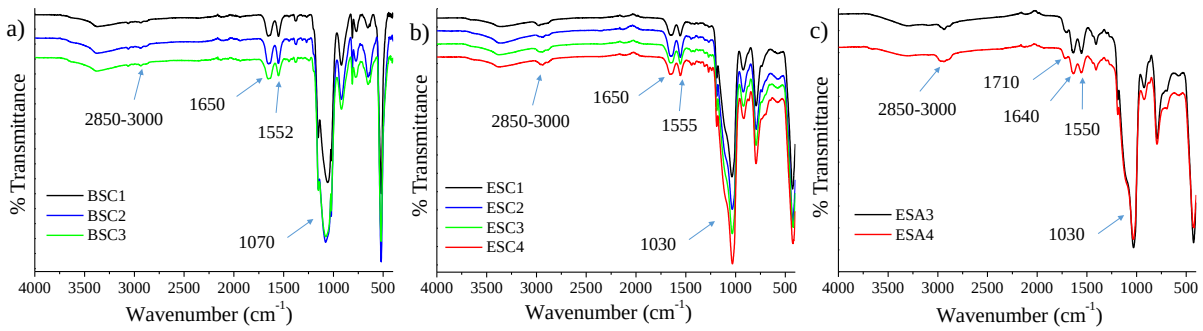

Figure S13. ATR-FTIR spectra of a) semicarbazide functionalized spherical nanoPMOs, b) semicarbazide functionalized nanoPMO nanorods, and c) carboxylic acid functionalized nanoPMO nanorods. In the case of semicarbazide functionalized nanoparticles, the characteristic bands for C=O stretching and N-H bending of the amide bond appear at around 1650 and 1553 cm^{-1}, respectively. In contrast, nanoPMOs functionalized with carboxylic acid similarly show amide bond bands at 1640 and 1550 cm^{-1}. Besides, the peak at 1710 cm^{-1} corresponds to the C=O starching of carboxylic groups. For all surface functionalized nanoparticles, the enhancement of the intensity of C-H stretching of methylene groups in the region of 2850-3000 cm^{-1} compared to as-synthesized nanoparticles indicates the successful surface modification of nanoparticles.

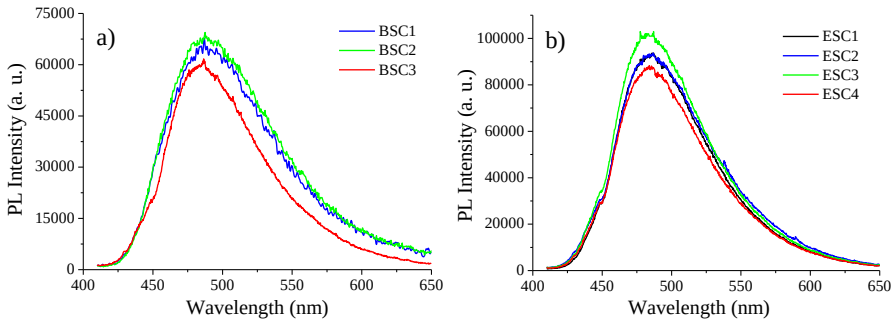

Figure S14. The fluorescence spectra of non-fluorescent fluorescamine molecules after incubation with several semicarbazide functionalized nanospheres (a) and nanorods (b) at basic conditions. The production of enhanced emission around 485 nm under excitation of 390 nm indicates the presence of primary amine groups on the surface of nanoparticles.

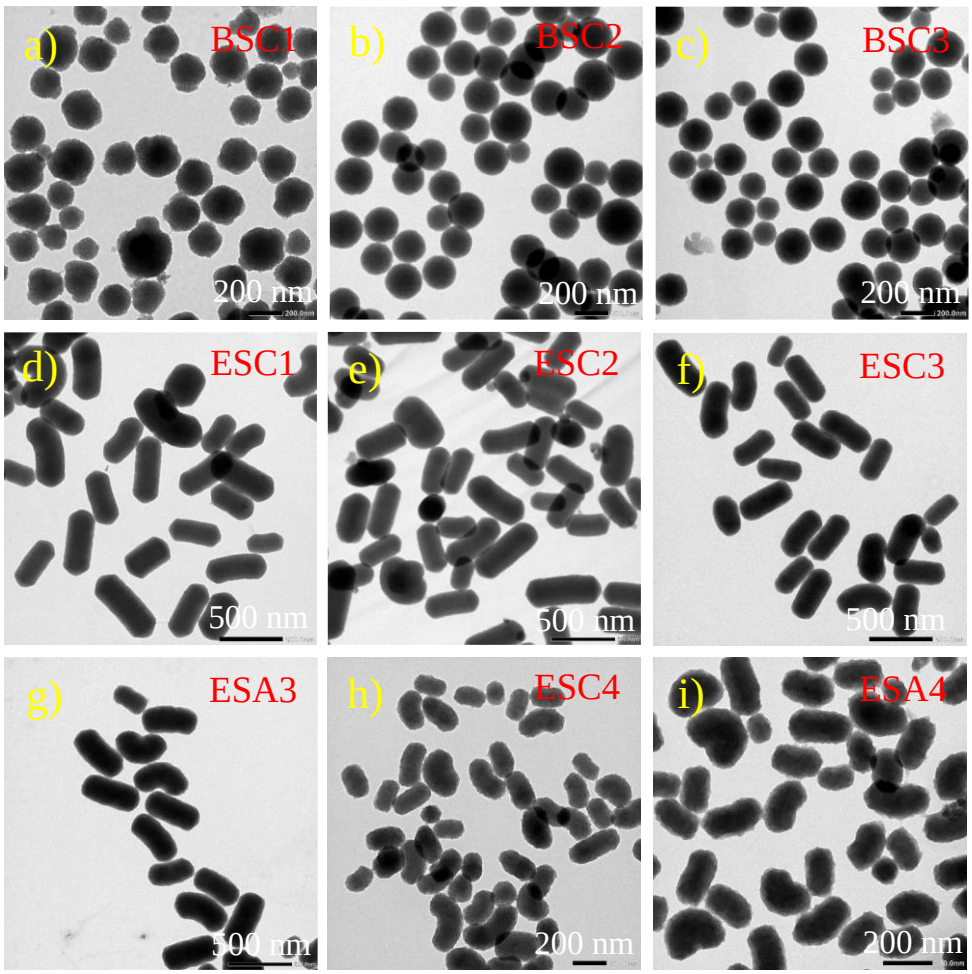

Figure S15. Representative TEM images of various surface functionalized nanoPMOs. a) BSC1 nanosphere, b) BSC2 nanosphere, c) BSC3 nanosphere, d) ESC1 nanorod, e) ESC2 nanorod, f) ESC3 nanorod, g) ESA3 nanorod, h) ESC4 nanorod, and i) ESA4 nanorod.

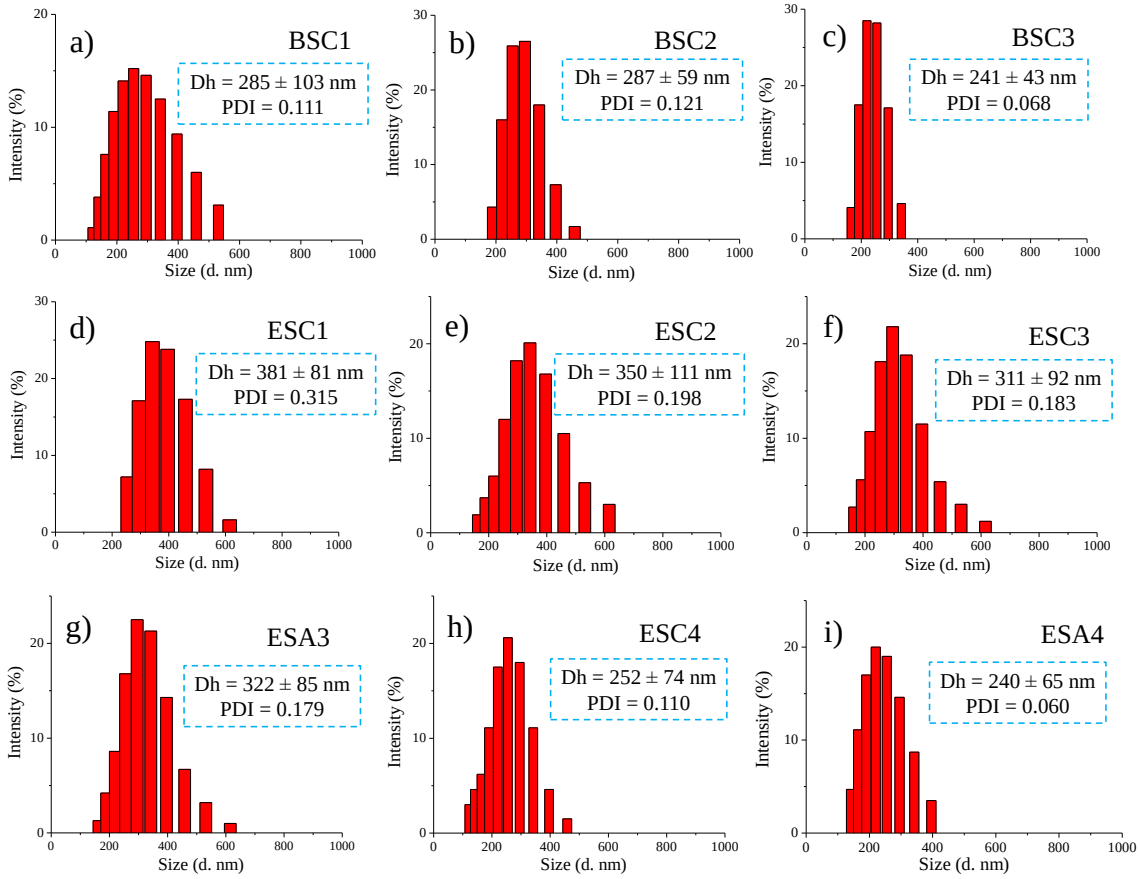

Figure S16. Hydrodynamic size distribution of various surface functionalized nanoPMOs measured by dynamic light scattering method. a) BSC1 nanosphere, b) BSC2 nanosphere, c) BSC3 nanosphere, d) ESC1 nanorod, e) ESC2 nanorod, f) ESC3 nanorod, g) ESA3 nanorod, h) ESC4 nanorod, and i) ESA4 nanorod. The inset of the histogram demonstrates their hydrodynamic size (Dh) and polydispersity index (PDI).

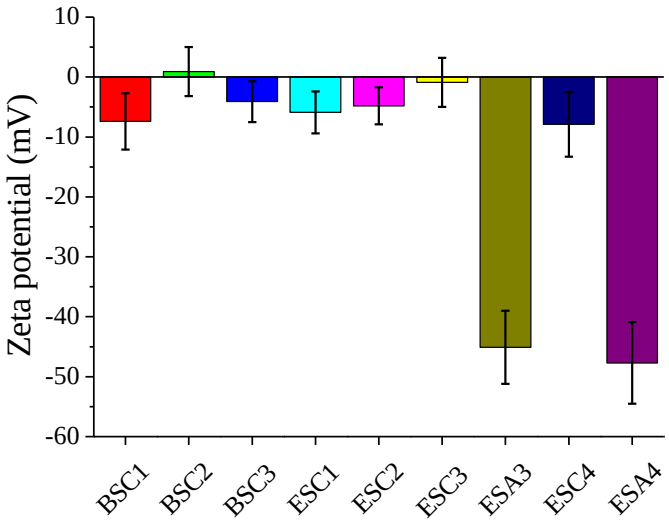

Figure S17. Zeta potentials of aqueous solution of various surface functionalized nanoPMOs.

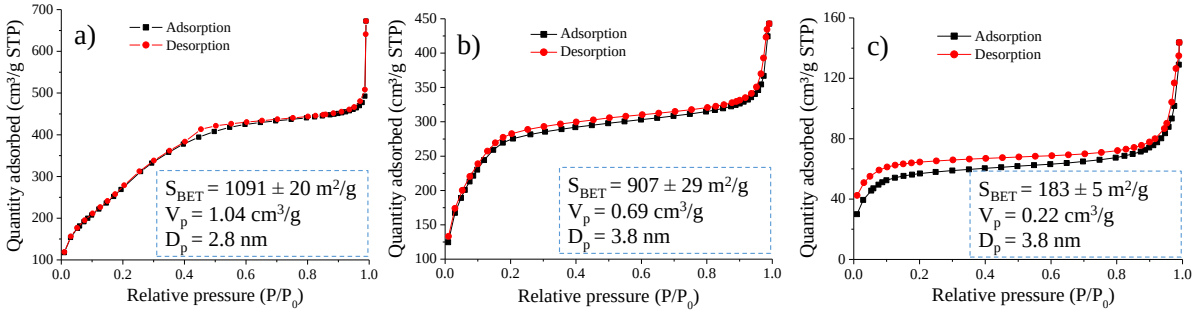

Figure S18. Nitrogen adsorption-desorption isotherms of a) semicarbazide functionalized EPMO (75/25) nanorod (ESC3), b) semicarbazide functionalized EPMO (60/40) nanorod (ESC4), and c) carboxylic acid functionalized EPMO (60/40) nanorod (ESA4). The insets show the value of the surface area (S_{BET}), pore volume (V_p), and pore diameter (D_p) of the corresponding mesoporous nanoparticles.

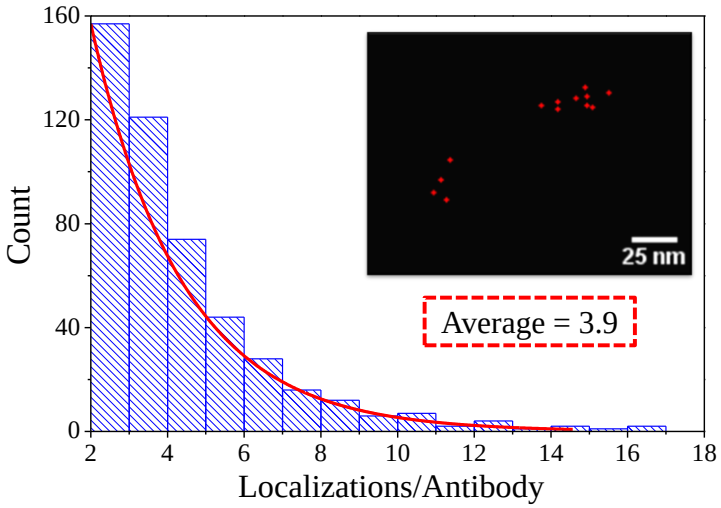

Figure S19. The distribution of localization number produced from Cy5 dye blinking *per* anti-M6PR antibody labeled with Cy5 dye. A representative dSTORM image is shown in the inset.

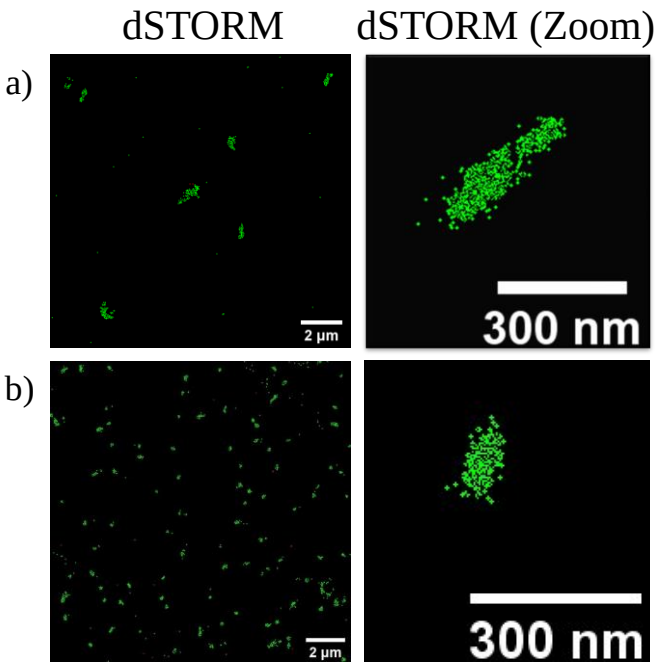

Figure S20. The dSTORM images of a) semicarbazide functionalized nanorod (ESC3) and b) purified carboxylic acid functionalized nanorod (ESA4) pre-incubated with antibody in absence of EDC/NHS. The dSTORM images are acquired at the same conditions as antibody conjugated nanoparticles.

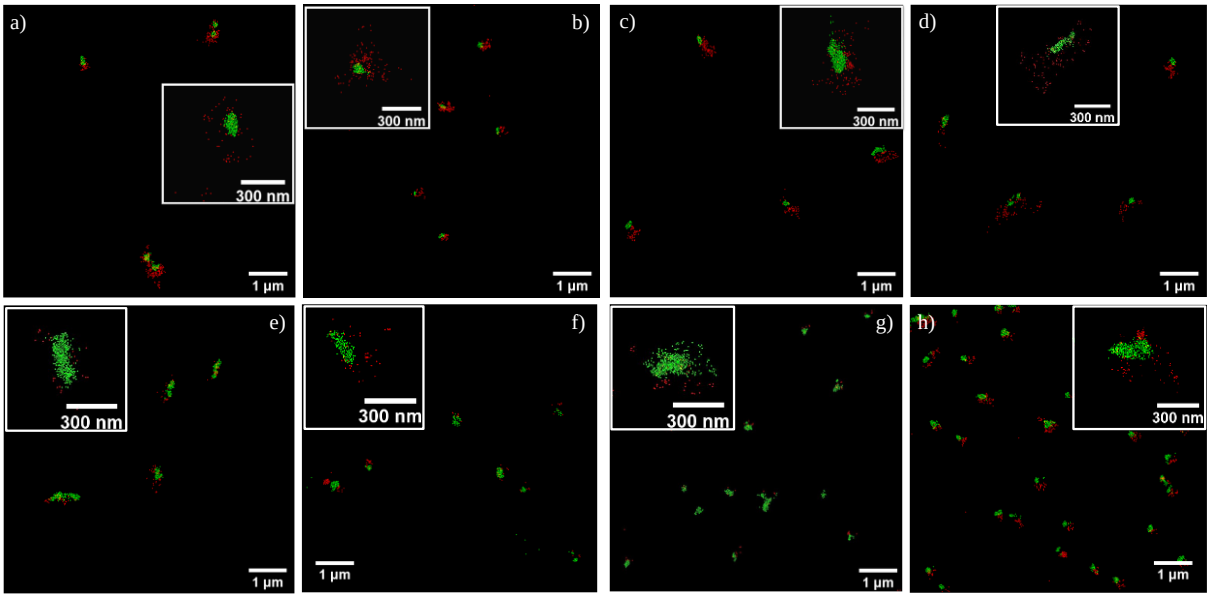

Figure S21. The dSTORM imaging of of antibody-conjugated nanoPMOs. Nanoparticles are presented in green, whereas antibody localizations are displayed in red. a) BAB1H, b) BAB2H, c) EAB1H, d) EAB2H, e) EAB3L, f) EBA3H*, g) EAB4L, and h) EBA4H*. The insets depict the zoom of dSTORM images, showing antibody conjugated individual nanoparticles.

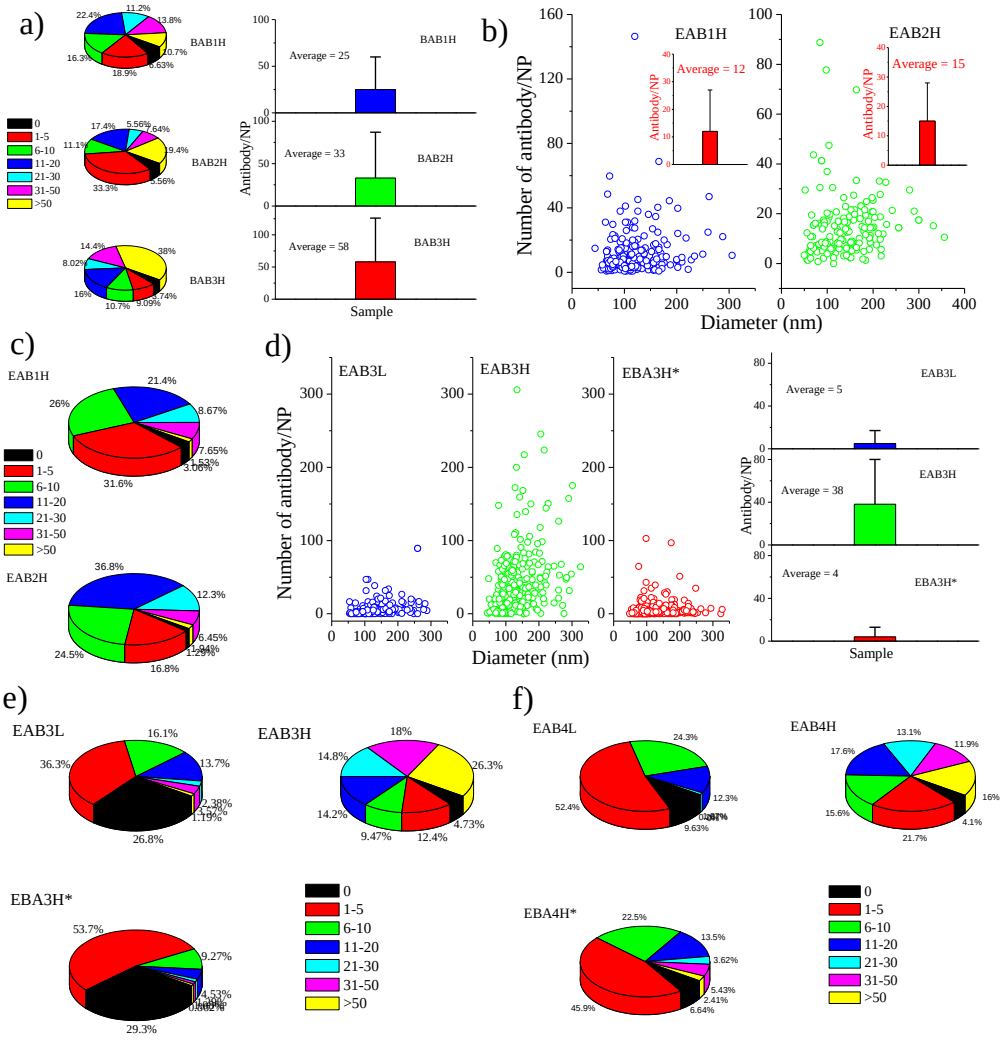

Figure S22. a) Pie chart showing the population of spherical nanoPMOs conjugated with a specific number of antibody (left side) and the average number of antibody *per* nanoparticle is presented for the corresponding samples (right side). b) The distribution of antibody numbers *per* nanoparticle of antibody conjugated nanorods, EAB1H and EAB2H measured by dSTORM analysis. The inset shows the average number of antibody *per* nanoparticle. c) Pie chart presenting the population of EAB1H and EAB2H nanorods conjugated with a specific number of antibody, d) The distribution of antibody numbers *per* nanoparticle of antibody conjugated ESC3 and ESA3 nanorods at different orientations and multivalency determined by dSTORM analysis (left side) and the average number of antibody *per* nanoparticle is presented for the corresponding samples (right side). e, f) Pie chart displaying the population of these nanorods, respectively conjugated with a specific number of antibody at different orientations and multivalency.

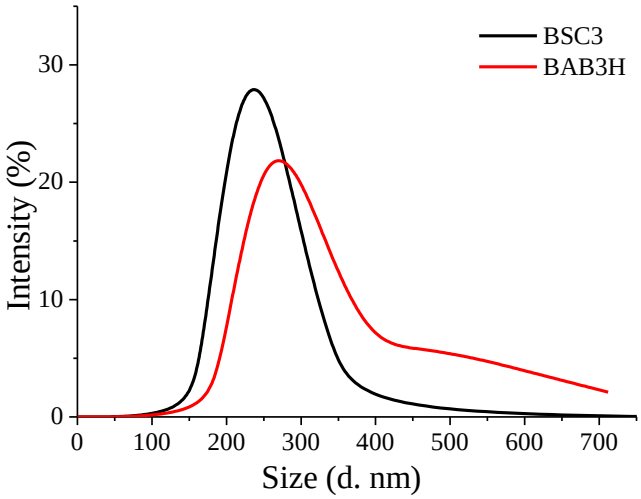

Figure S23. The hydrodynamic size of pre (BSC3) and post (BAB3H) antibody conjugated spherical nanoparticles as determined by the dynamic light scattering method. The average diameter of BSC3 nanoparticles increases from 241 ± 43 nm to 330 ± 126 nm after antibody conjugation.

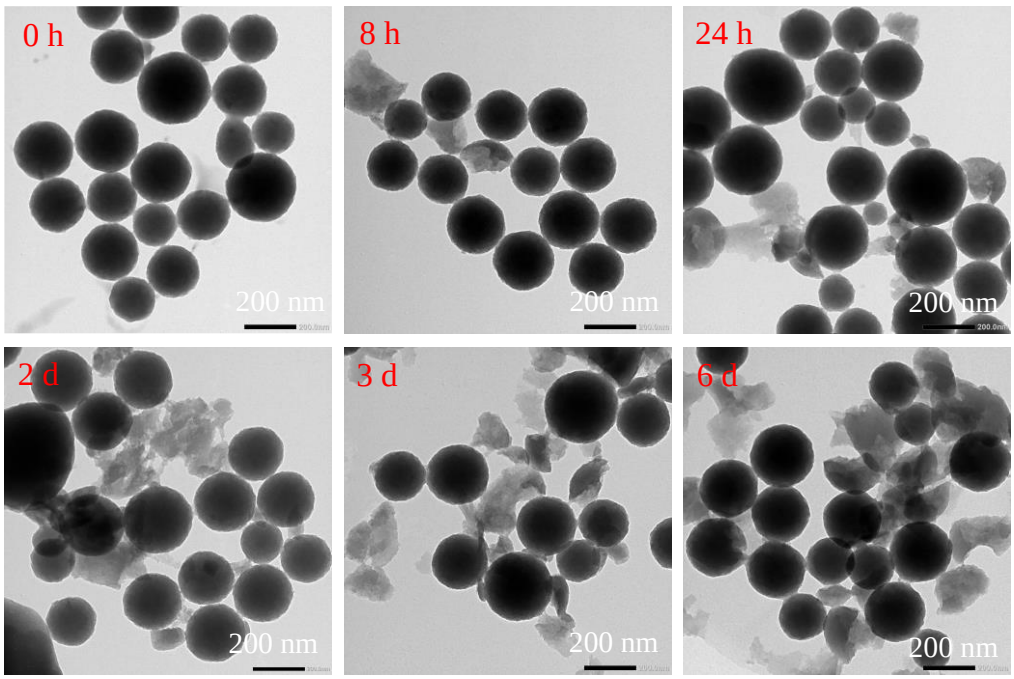

Figure S24. Representative TEM images of biodegradable BSC2 nanosphere after incubation in 10 mM phosphate buffered solution (pH 7.4) containing 10 mM GSH for different times.

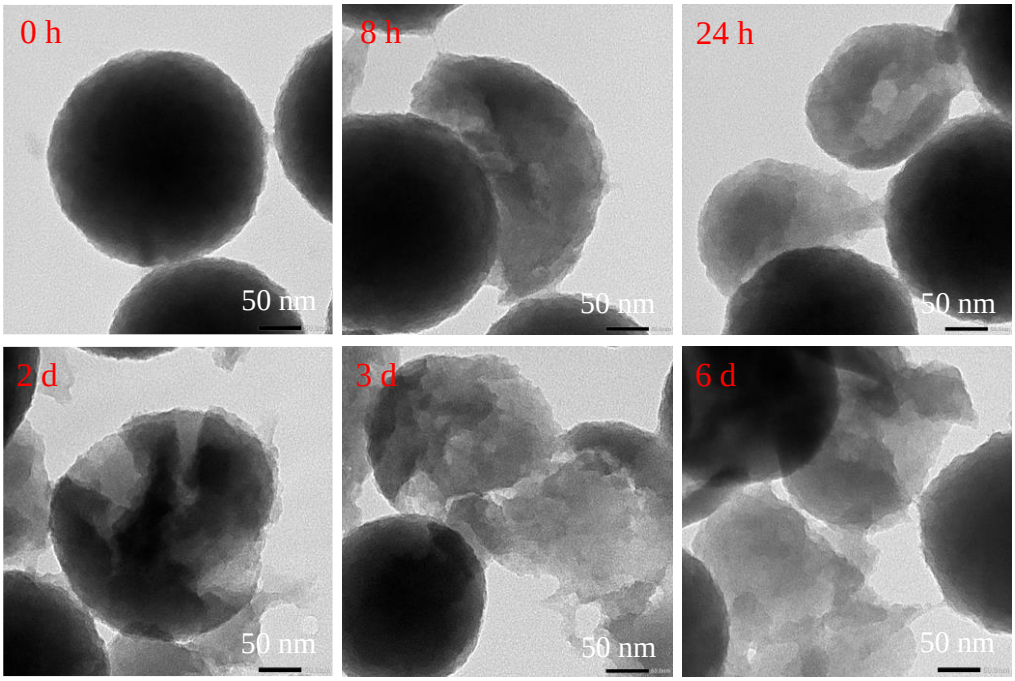

Figure S25. Representative TEM images at higher magnification of biodegradable BSC2 nanosphere after incubation in 10 mM phosphate buffered solution (pH 7.4) containing 10 mM GSH for different times.

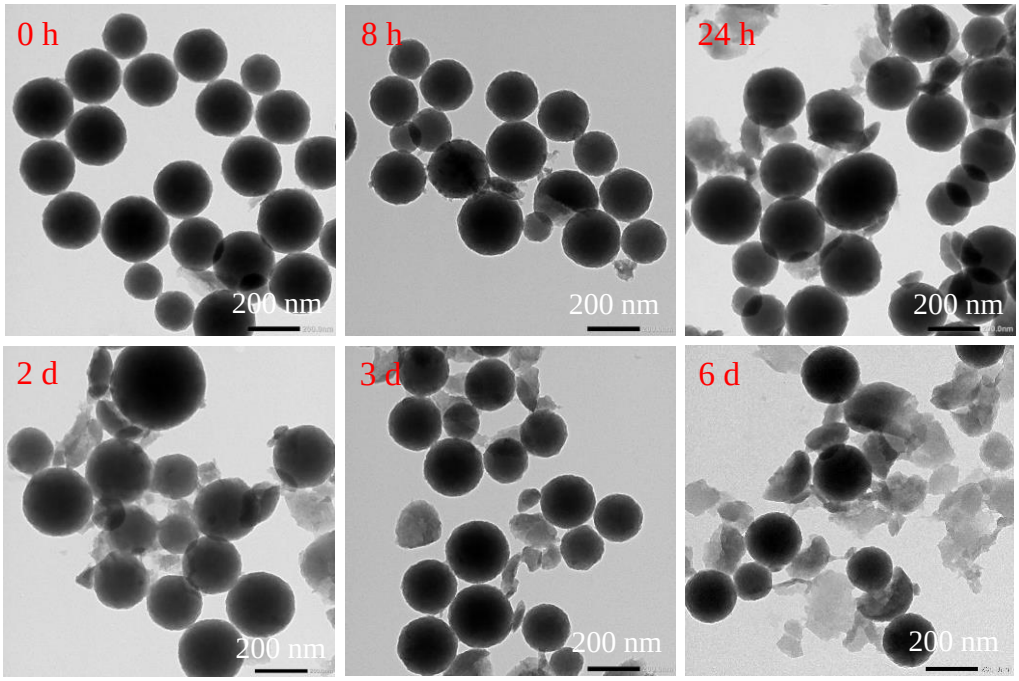

Figure S26. Representative TEM images of biodegradable BSC3 nanosphere after incubation in 10 mM phosphate buffered solution (pH 7.4) containing 10 mM GSH for different times.

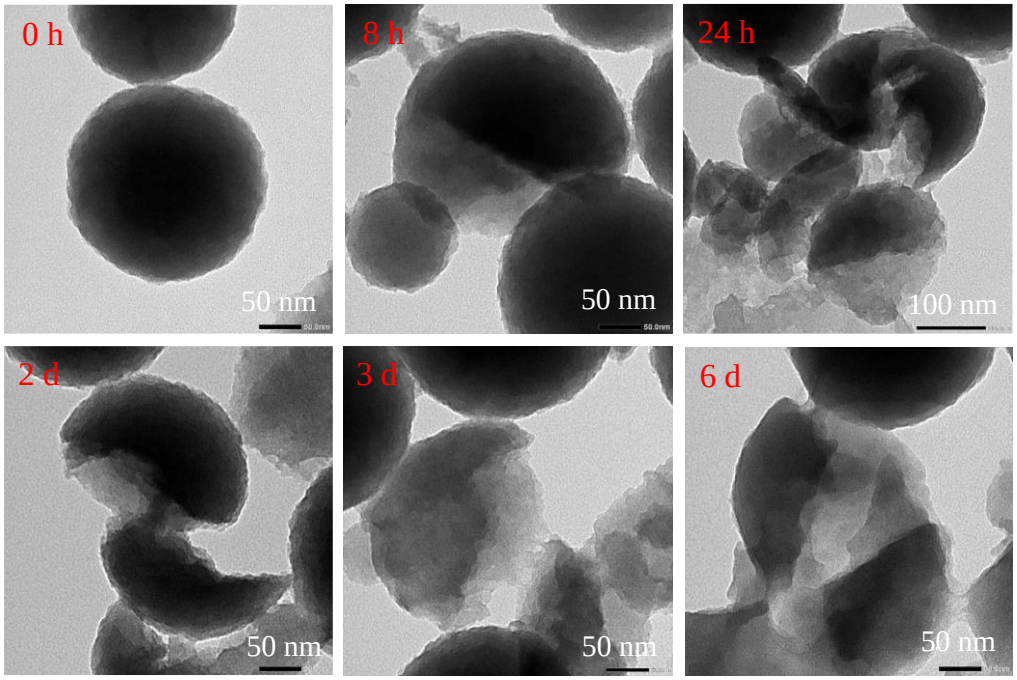

Figure S27. Representative TEM images at higher magnification of biodegradable BSC3 nanosphere after incubation in 10 mM phosphate buffered solution (pH 7.4) containing 10 mM GSH for different times.

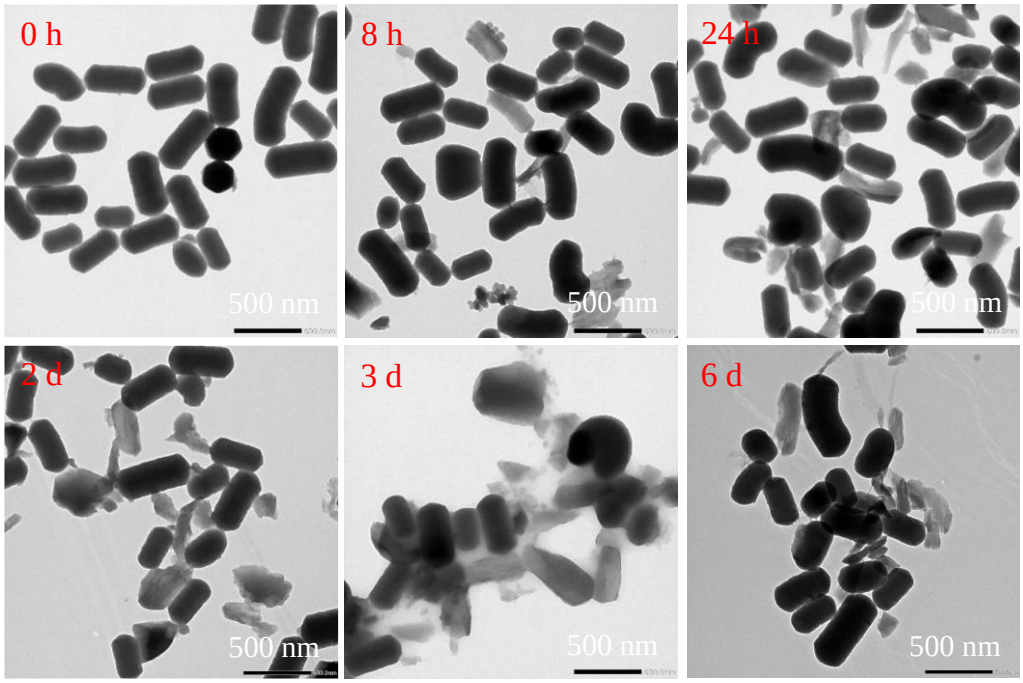

Figure S28. Representative TEM images of biodegradable ESC2 nanorod after incubation in 10 mM phosphate buffered solution (pH 7.4) containing 10 mM GSH for different times.

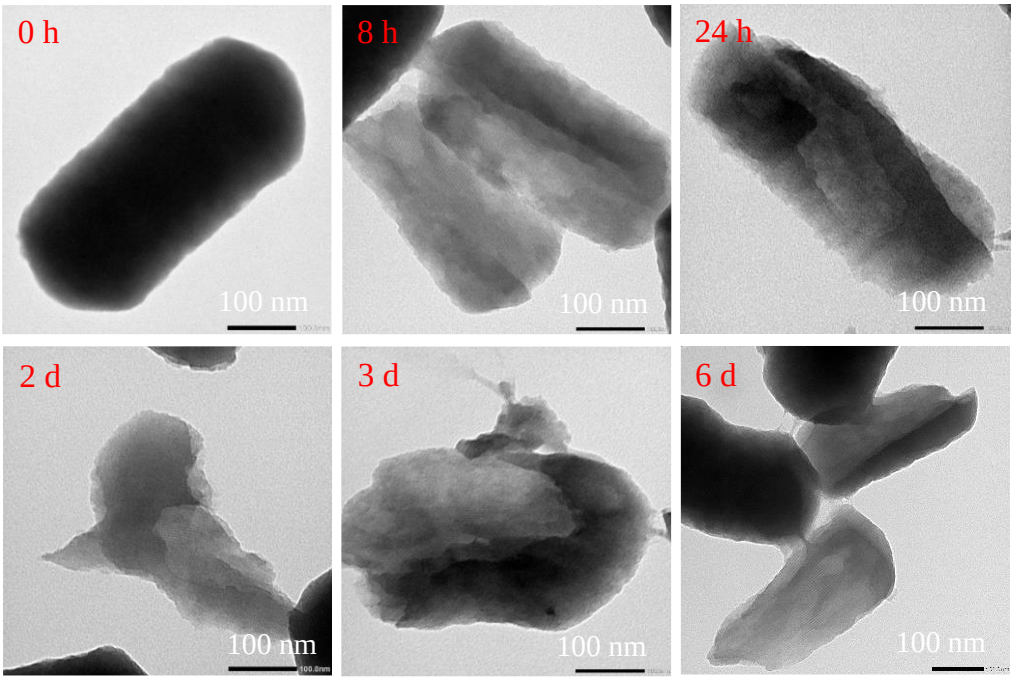

Figure S29. Representative TEM images at higher magnification of biodegradable ESC2 nanorod after incubation in 10 mM phosphate buffered solution (pH 7.4) containing 10 mM GSH for different times.

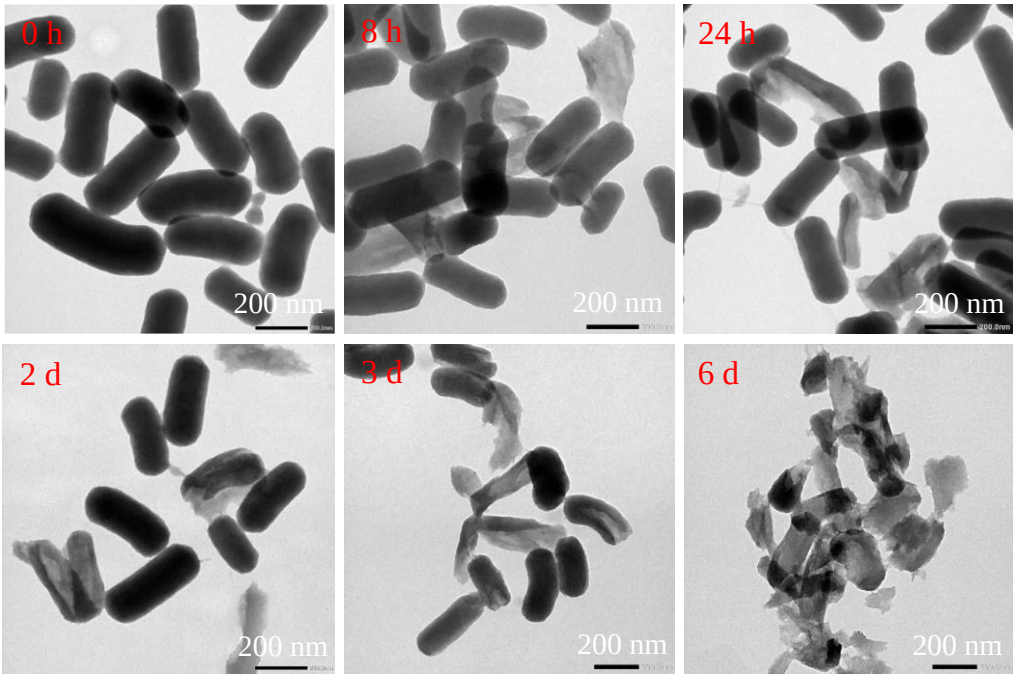

Figure S30. Representative TEM images of biodegradable ESC3 nanorod after incubation in 10 mM phosphate buffered solution (pH 7.4) containing 10 mM GSH for different times.

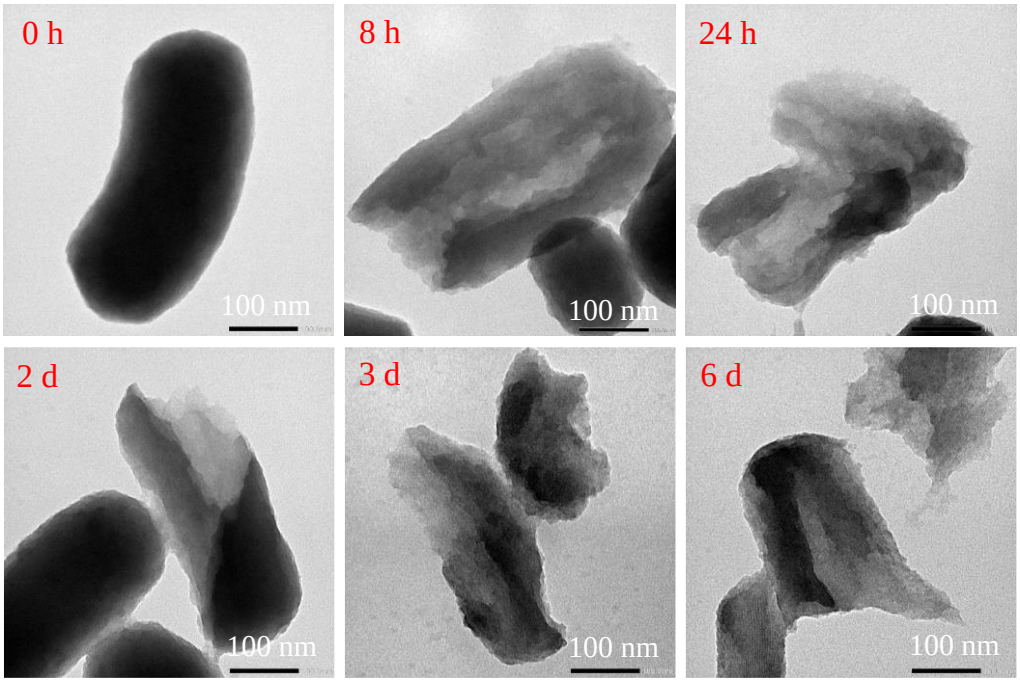

Figure S31. Representative TEM images at higher magnification of biodegradable ESC3 nanorod after incubation in 10 mM phosphate buffered solution (pH 7.4) containing 10 mM GSH for different times.

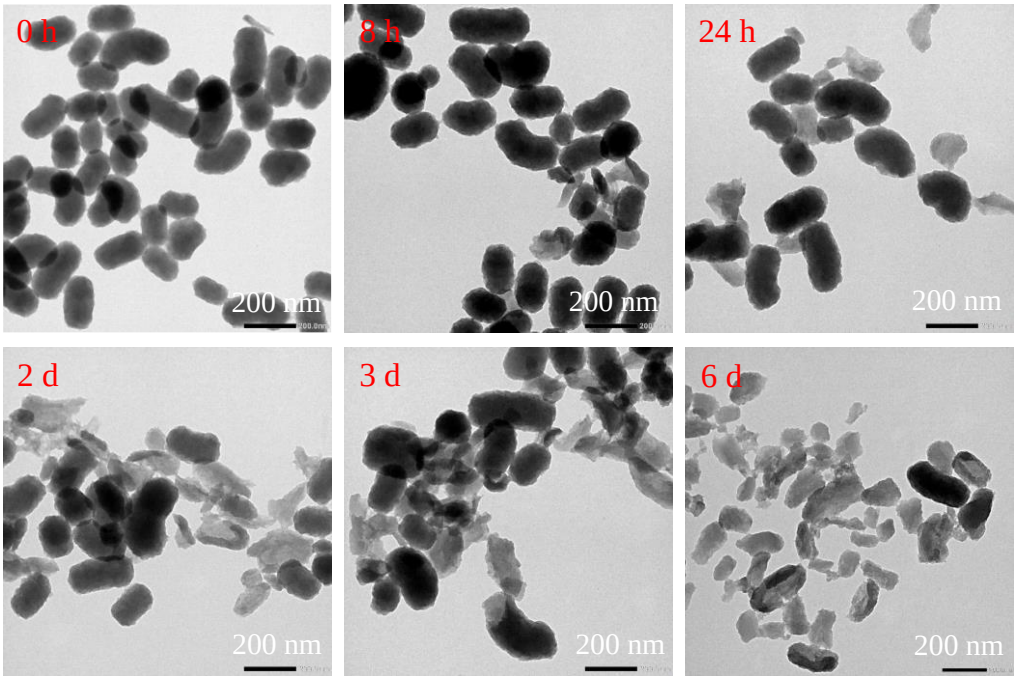

Figure S32. Representative TEM images of biodegradable ESC4 nanorod after incubation in 10 mM phosphate buffered solution (pH 7.4) containing 10 mM GSH for different times.

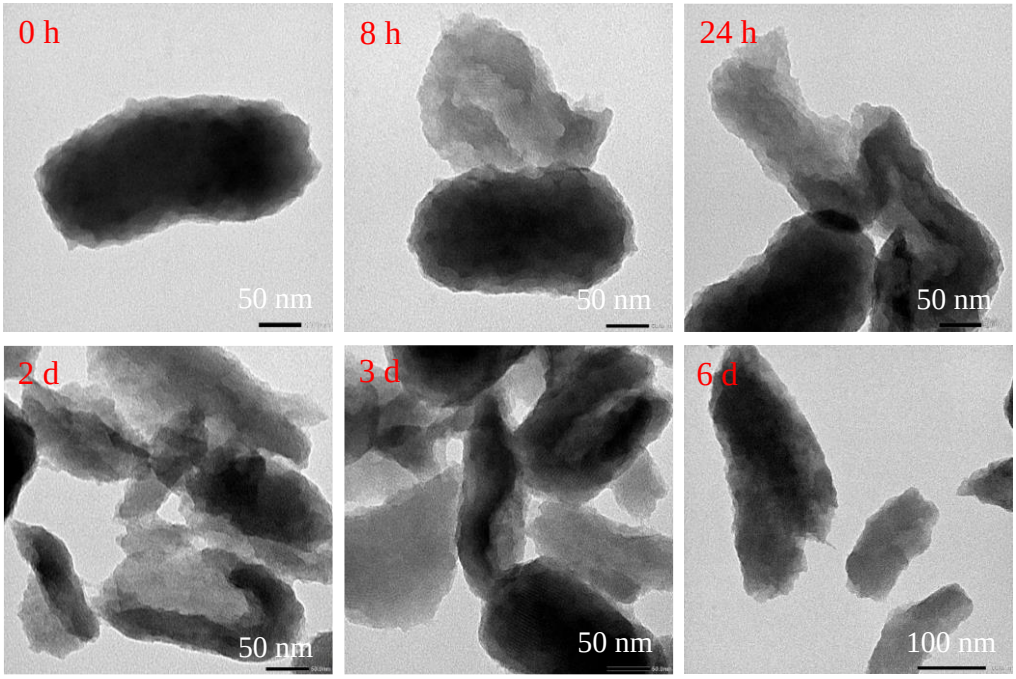

Figure S33. Representative TEM images at higher magnification of biodegradable ESC4 nanorod after incubation in 10 mM phosphate buffered solution (pH 7.4) containing 10 mM GSH for different times.

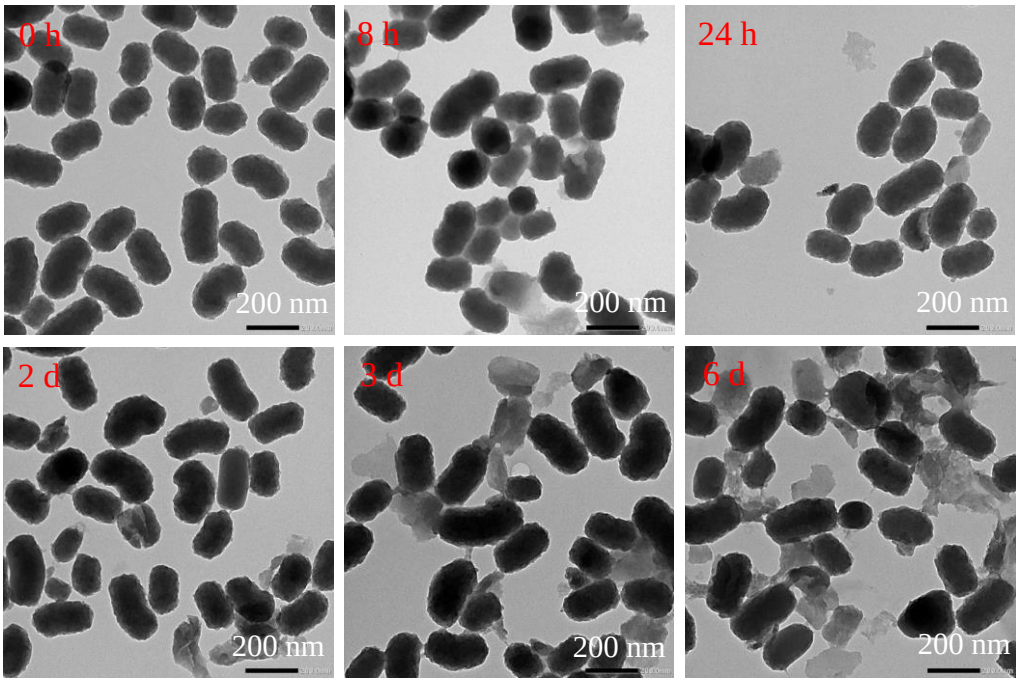

Figure S34. Representative TEM images of biodegradable ESA4 nanorod after incubation in 10 mM phosphate buffered solution (pH 7.4) containing 10 mM GSH for different times.

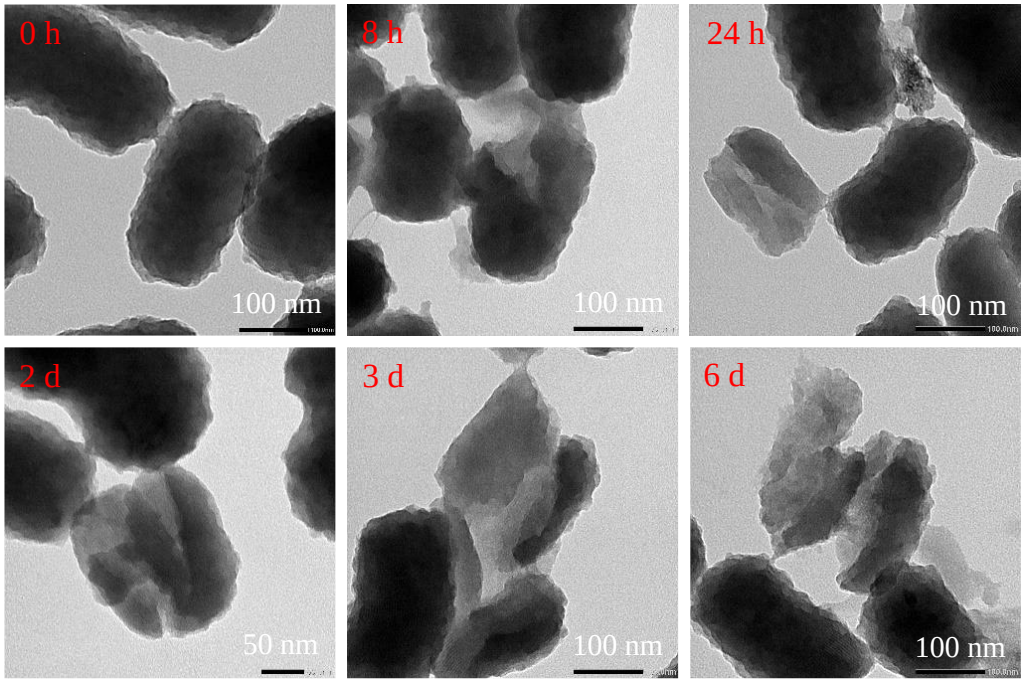

Figure S35. Representative TEM images at higher magnification of biodegradable ESA4 nanorod after incubation in 10 mM phosphate buffered solution (pH 7.4) containing 10 mM GSH for different times.

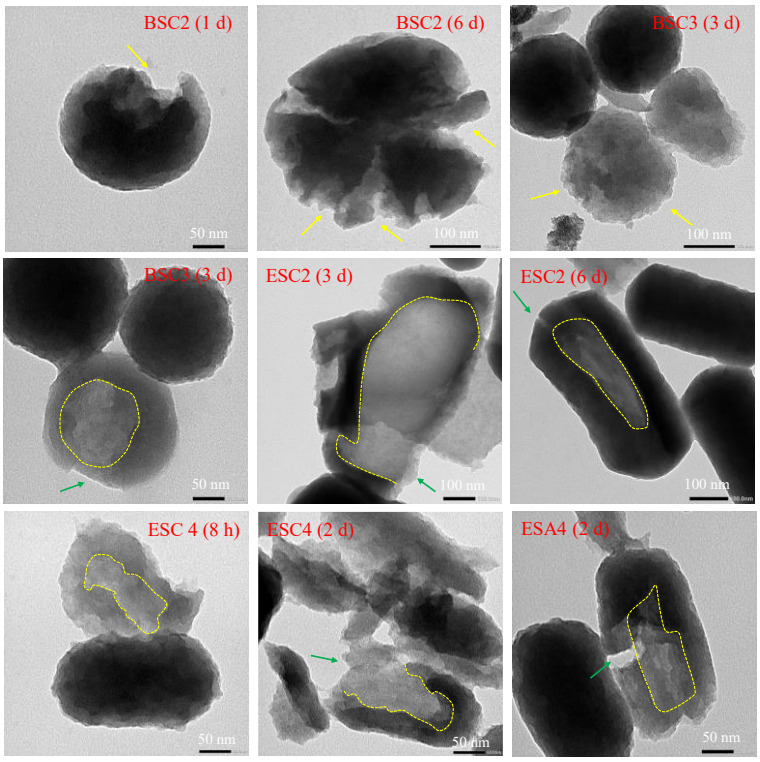

Figure S36. Representative TEM images at higher magnification of various degraded nanoPMOs after incubation with 10 mM glutathione solution in phosphate buffer (10 mM, pH 7.4) at different times. The surface erosion of nanoPMOs caused by external glutathione is shown by yellow-colored arrows. The region of hollow space produced via cleaving polysulfide network in the core by diffused glutathione is marked by yellow-colored dotted lines. The green-colored arrows represent the degraded part of nanoparticles containing hollow structures.

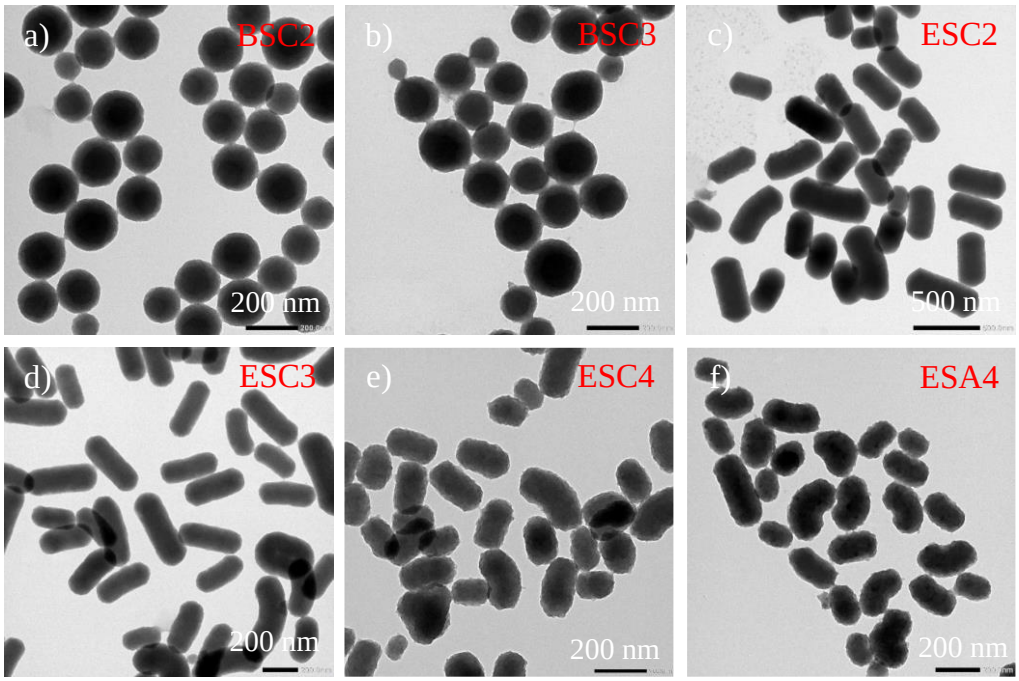

Figure S37. Representative TEM images of several biodegradable nanoPMOs after 6 days incubation in phosphate buffered solution (10 mM, pH 7.4) containing 10 µM GSH. a) BSC2, b) BSC3, c) ESC2, d) ESC3, e) ESC4, and f) ESA4.

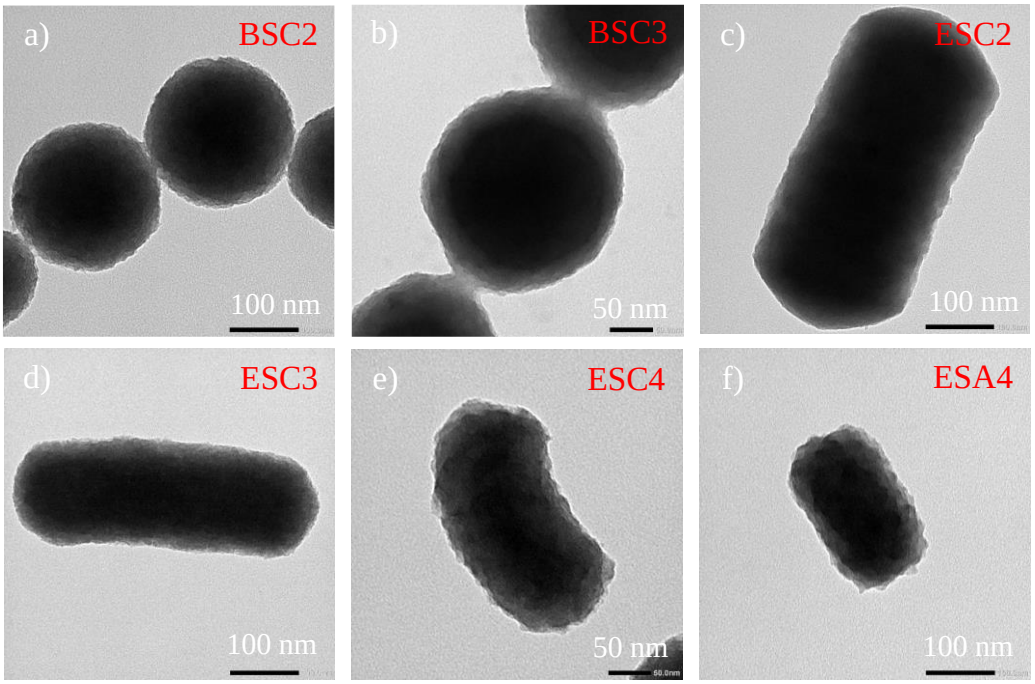

Figure S38. Representative TEM images at higher magnification of several biodegradable nanoPMOs after 6 days incubation in phosphate buffered solution (10 mM, pH 7.4) containing 10 µM GSH. a) BSC2, b) BSC3, c) ESC2, d) ESC3, e) ESC4, and f) ESA4.

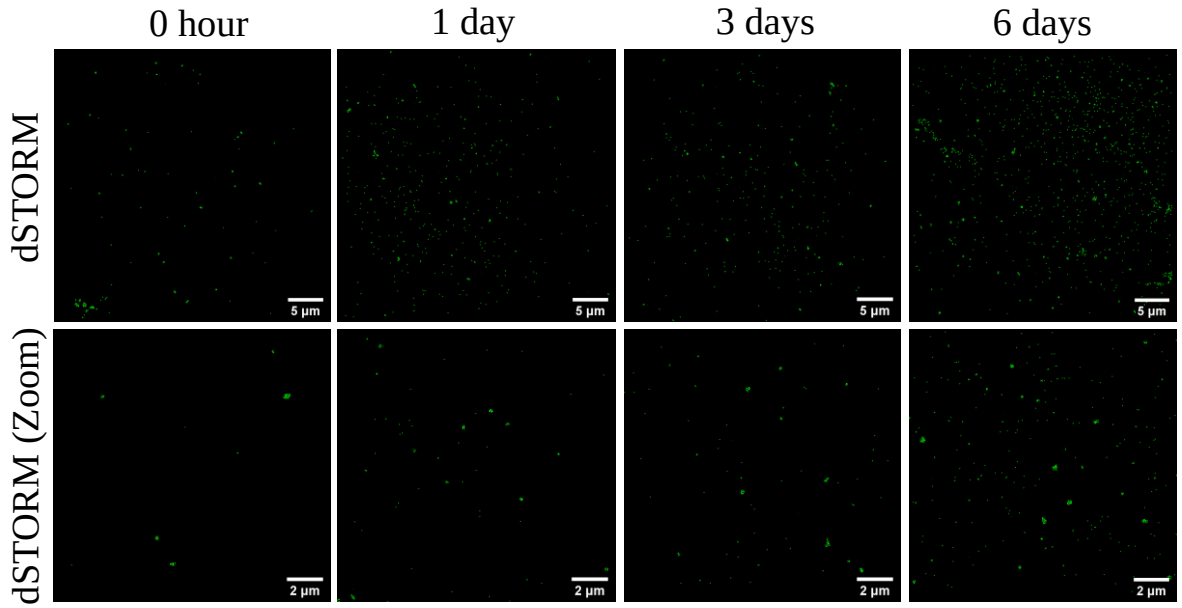

Figure S39. dSTORM imaging of biodegradable BSC2 nanosphere after incubation for different times in 10 mM phosphate buffered solution (pH 7.4) containing 10 mM GSH.

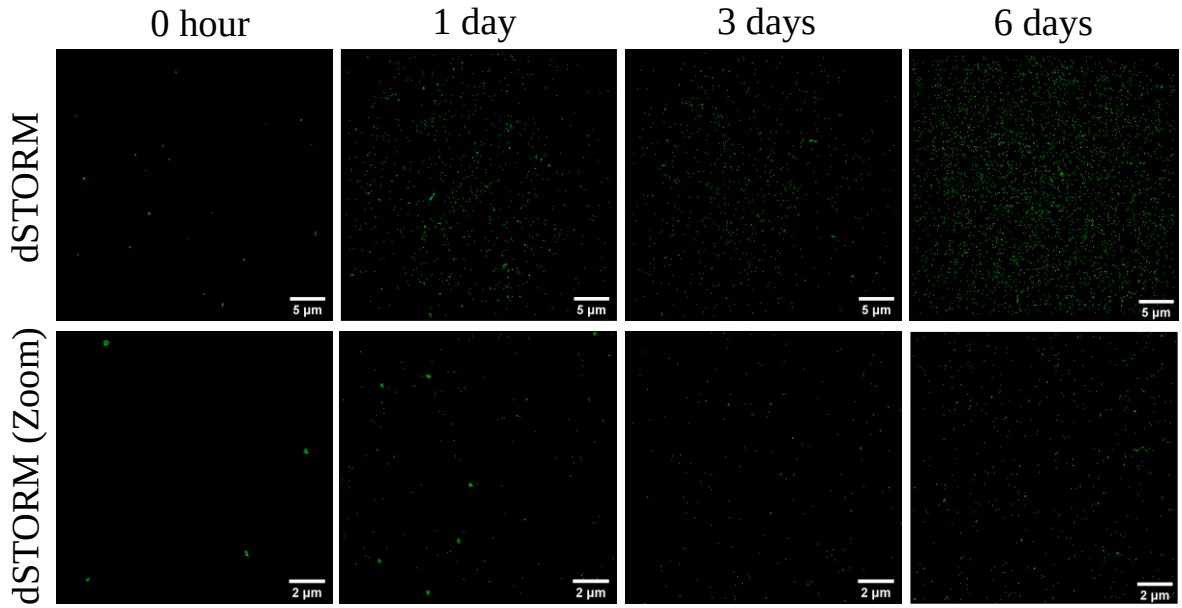

Figure S40. dSTORM imaging of biodegradable BSC3 nanosphere after incubation for different times in 10 mM phosphate buffered solution (pH 7.4) containing 10 mM GSH.

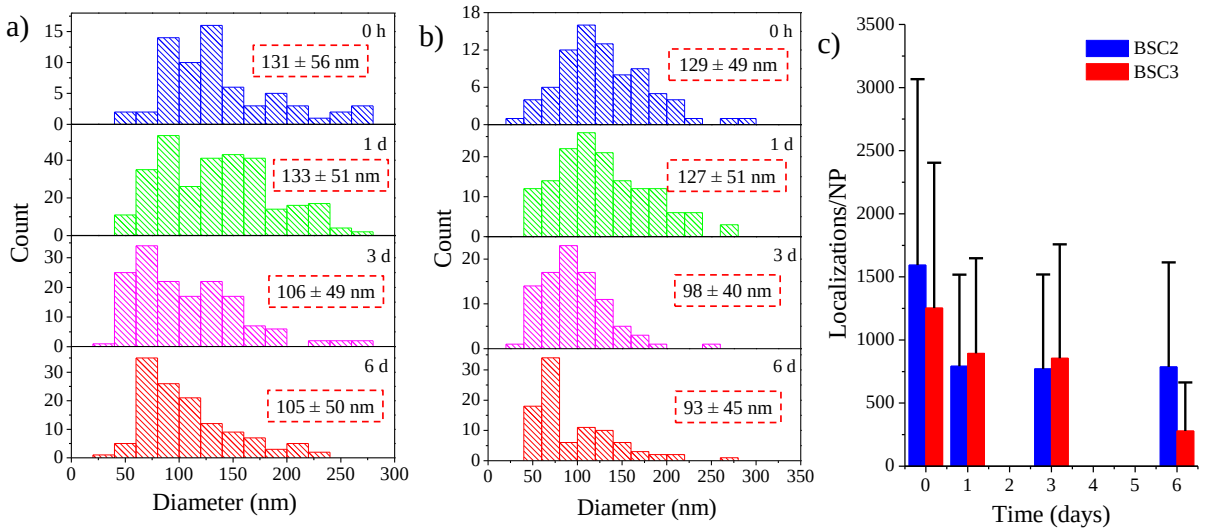

Figure S41. The optical size distribution histogram of a) BSC2 and b) BSC3 nanosphere after different time incubation with a phosphate-buffered solution containing 10 mM glutathione measured by dSTORM analysis. The inset display the calculated average optical diameter of degraded nanoparticles. c) The localization number per nanoparticle for BSC2 and BSC3 nanosphere at different incubation periods with 10 mM glutathione solution.

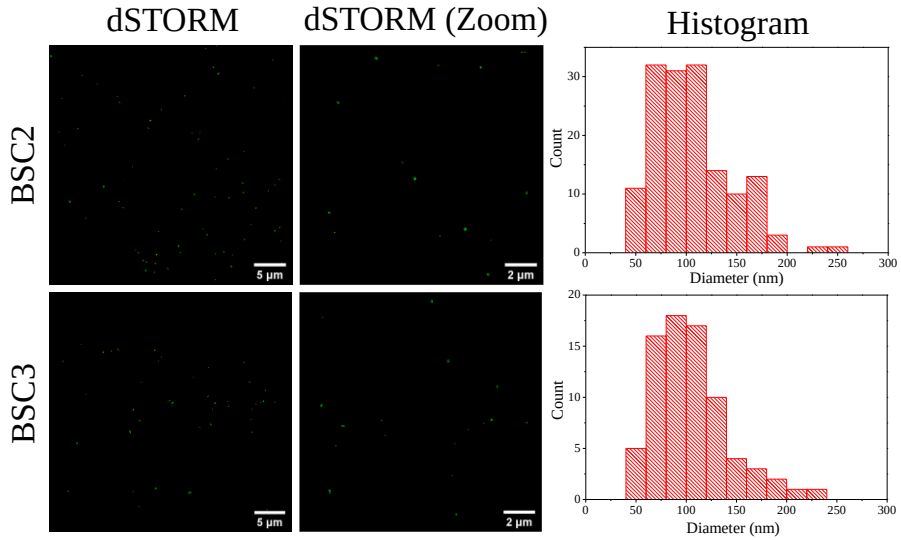

Figure S42. dSTORM imaging of biodegradable spherical nanoPMOs after 6 days incubation with 10 μM GSH solution in phosphate buffer (10 mM, pH 7.4) and their corresponding optical size distribution histogram.

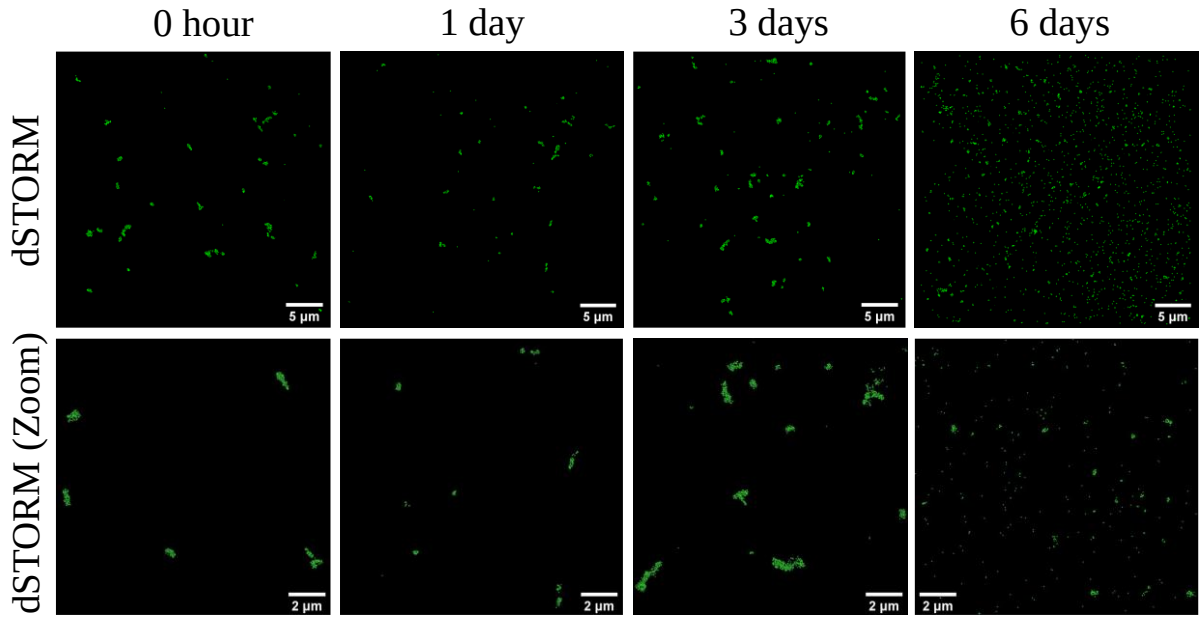

Figure S43. dSTORM imaging of biodegradable ESC2 nanorod incubated with 10 mM GSH in phosphate buffered solution (10 mM, pH 7.4) for varying times.

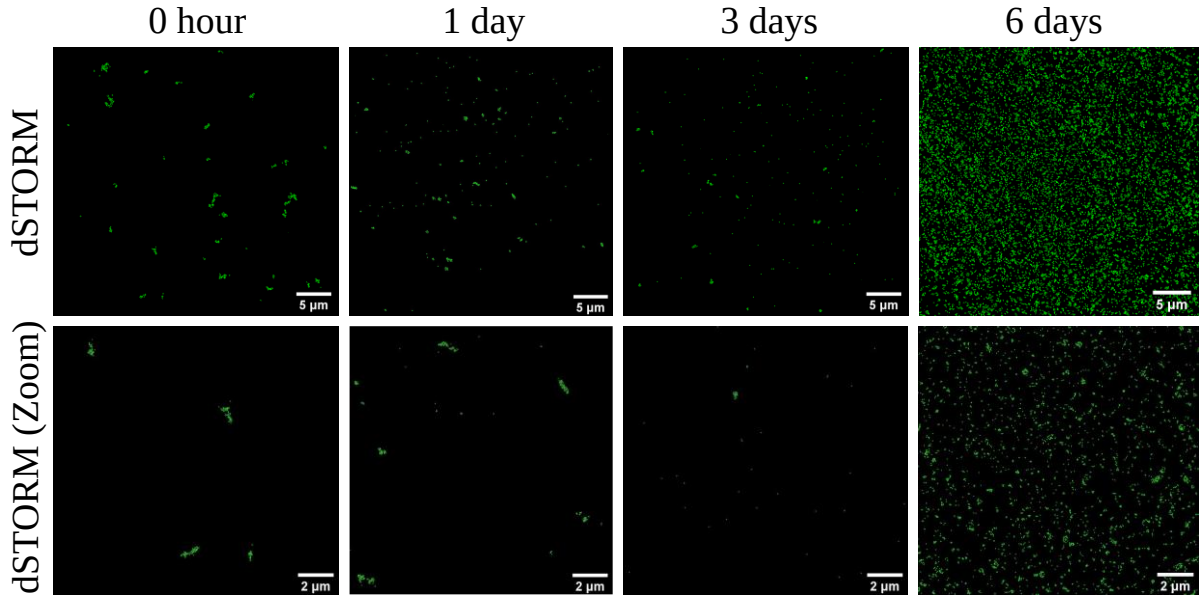

Figure S44. dSTORM imaging of biodegradable ESC3 nanorod incubated with 10 mM GSH in phosphate buffered solution (10 mM, pH 7.4) for varying times.

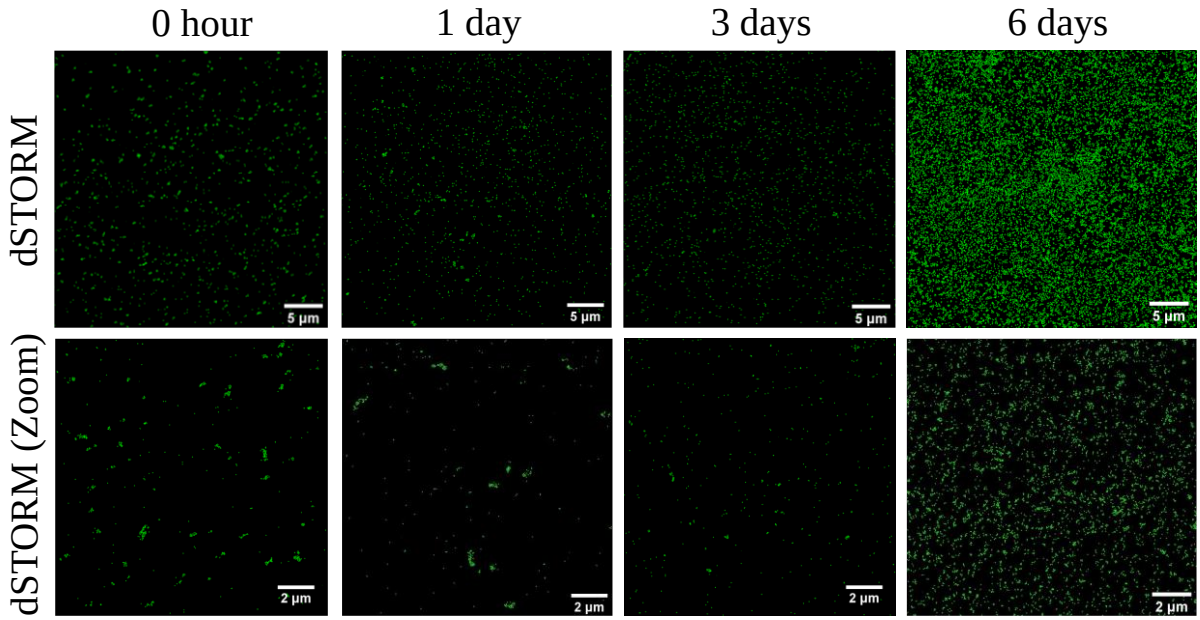

Figure S45. dSTORM imaging of biodegradable ESC4 nanorod incubated with 10 mM GSH in phosphate buffered solution (10 mM, pH 7.4) for varying times.

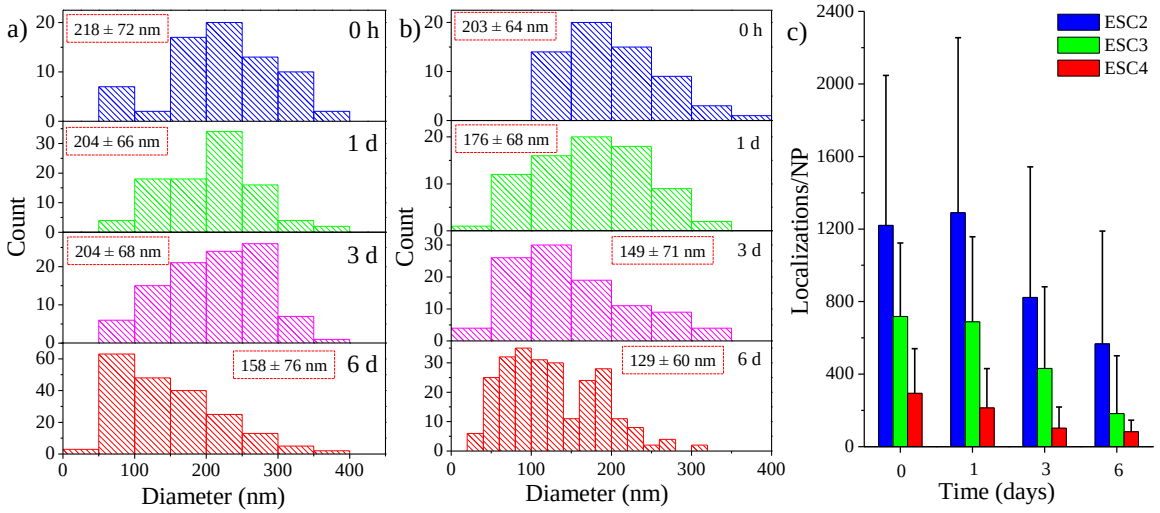

Figure S46. a, b) The optical size distribution histograms of the ESC2 and ESC3 nanorods, respectively after different incubation times with 10 mM glutathione in phosphate-buffered solution. The inset display the calculated average optical diameter of degraded nanoparticles. c) The variation of localization number per nanoparticle for these nanorods as a result of degradation by 10 mM glutathione solution at different incubation periods.

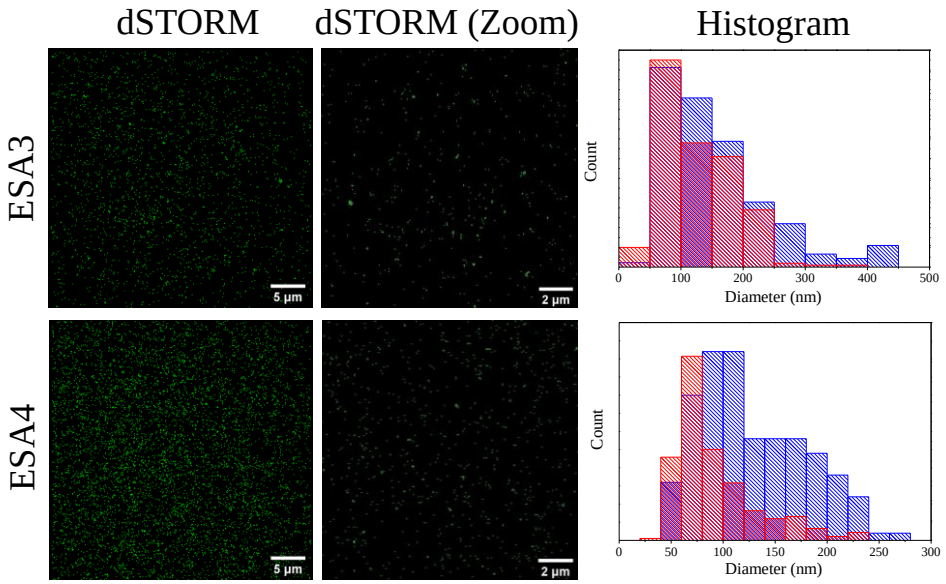

Figure S47. dSTORM imaging of carboxylic acid functionalized nanorods, ESA3 and ESA4 after incubation in 10 mM GSH solution in phosphate buffer (10 mM, pH 7.4) for 6 days and their corresponding optical size distribution histogram (red) in comparison to the histogram of their pristine nanorods (blue). The results demonstrate that ESA4 nanorods become more degradable than ESA3 nanorods due to the presence of high levels of disulfide bonds.

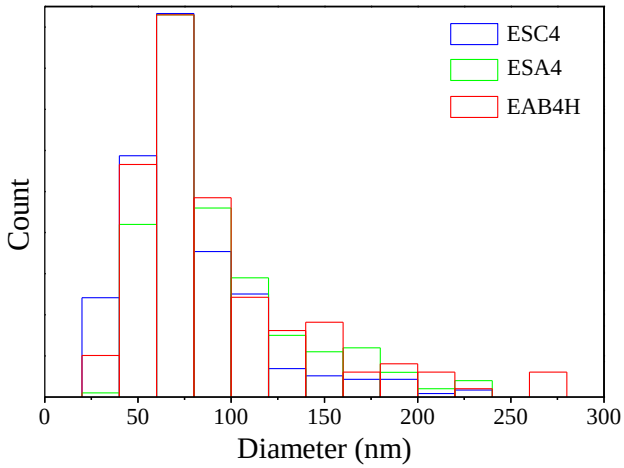

Figure S48. The optical size distribution of degraded EPMO (60/40) nanorods with different surface functionality such as ESC4, ESA4, and EAB4H nanorods in response to 10 mM GSH in phosphate buffer (10 mM, pH 7.4) after 6 days. The average optical diameter of degraded ESC4, ESA4, and EAB4H nanorods is 75 ± 35 nm, 91 ± 40 nm, and 92 ± 49 nm, respectively, showing the effect of surface chemistry on the degradation.

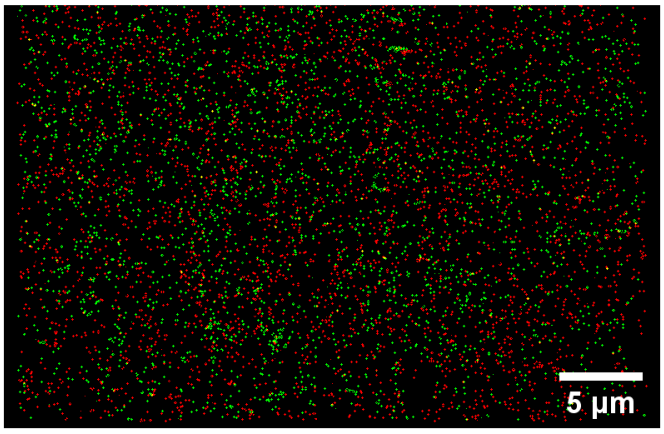

Figure S49. dSTORM imaging of oriented antibody conjugated ESC4 nanorod (EAB4H) after 6 days incubation with 10 mM GSH in phosphate buffer (10 mM, pH 7.4). The green and red colors represent the nanoparticles and antibodies, respectively.

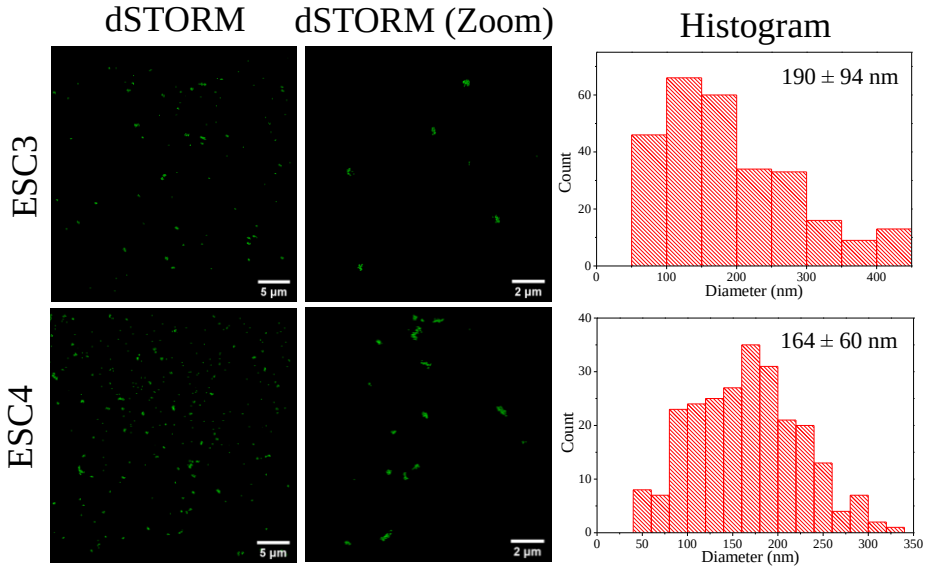

Figure S50. dSTORM imaging of biodegradable nanoPMO nanorods functionalized with semicarbazide groups after 6 days incubation with 10 µM GSH solution in phosphate buffer (10 mM, pH 7.4) and their corresponding optical size distribution histogram. The inset of the histogram shows the average optical diameter of nanorods which is close to the value of pristine nanoparticles.

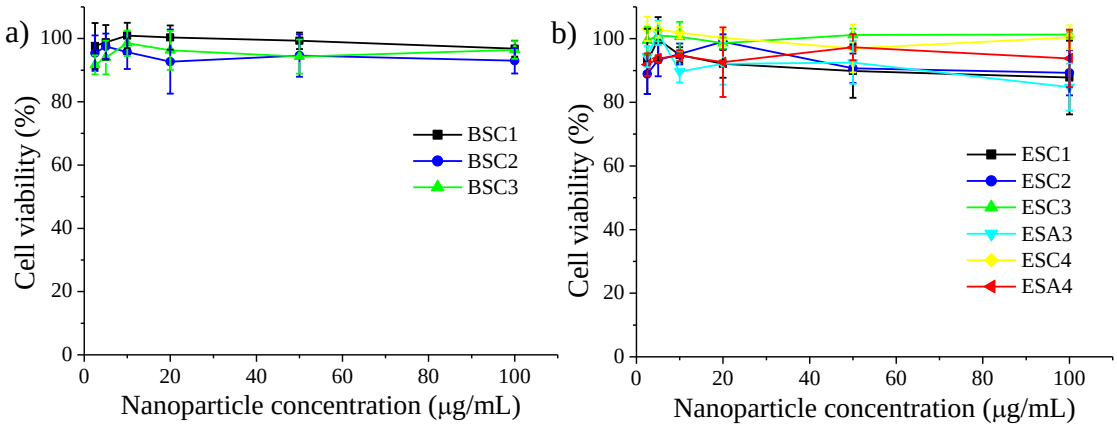

Figure S51. *In vitro* cytotoxicity of a) various functionalized spherical nanoPMOs and b) several nanoPMO nanorods with different surface functionality after 24 h incubation with prostate cancer LNCaP cells.

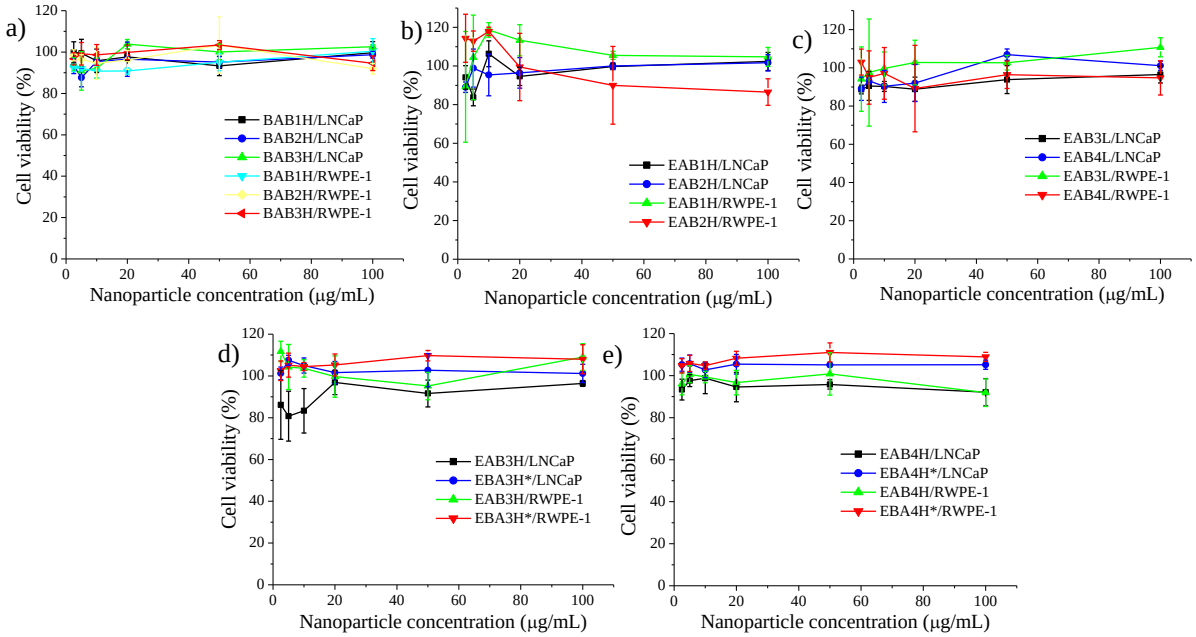

Figure S52. *In vitro* cytotoxicity of a) various antibody conjugated spherical nanoPMOs and b-e) several nanoPMO nanorods conjugated with antibody in different ways after 24 h incubation at different nanoparticle concentrations with prostate cancer LNCaP and healthy RWPE-1 cells.

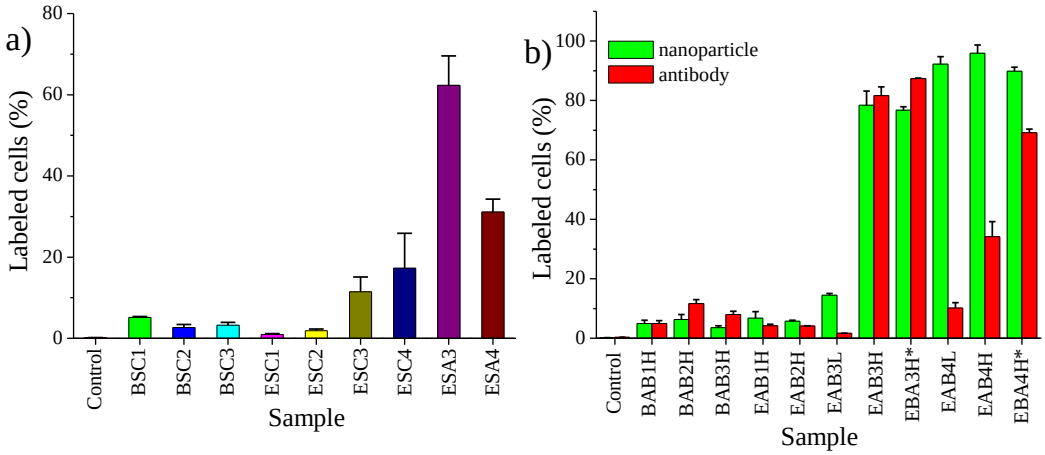

Figure S53. The quantification of fluorescent nanoPMOs labeled prostate cancer LNCaP cells after 6 h incubation with different a) non-conjugated nanoPMOs and b) antibody conjugated nanoPMOs by flow cytometry. Data are presented as mean ± SD of two independent experiments.

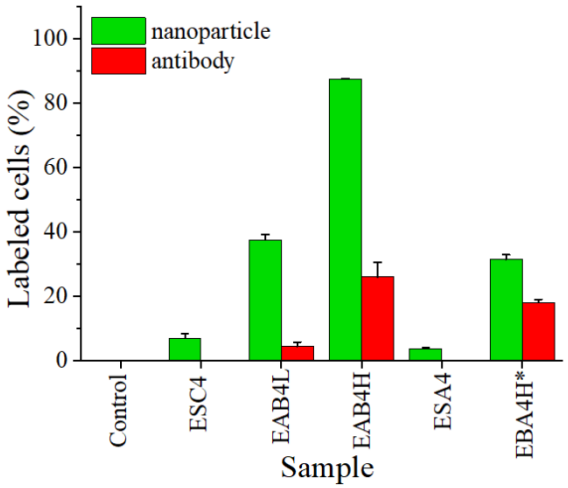

Figure S54. The quantification of fluorescent nanoPMOs nanorods labeled human rhabdomyosarcoma Rh30 cells showing M6PR overexpression after 6 h incubation with different non-conjugated nanoPMOs and antibody conjugated nanoPMOs by flow cytometry. Data are presented as mean ± SD of two independent experiments.

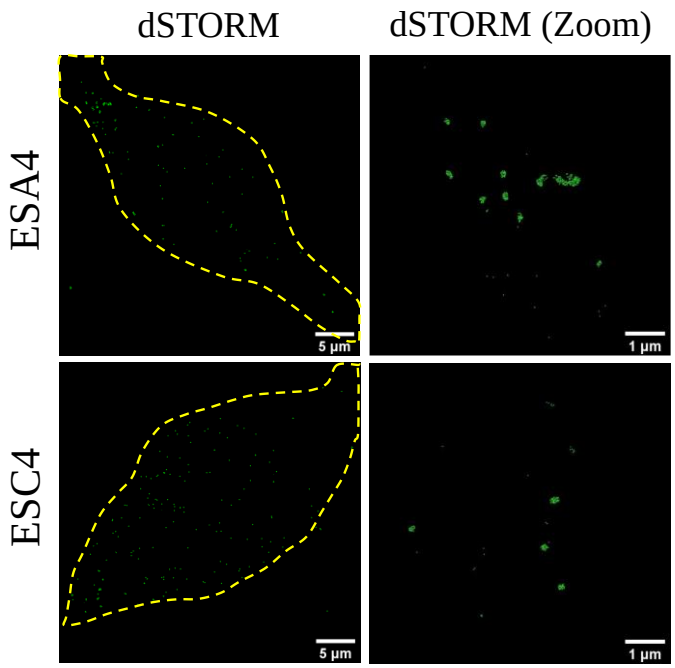

Figure S55. dSTORM imaging of prostate cancer LNCaP cells labeled with carboxylic acid functionalized nanoPMO nanorod (ESA4) and semicarbazide functionalized nanoPMO nanorod (ESC4) after 6 h incubation of nanoparticles at a final concentration of 6 µg/mL. The results suggest that both nanoparticles have low nonspecific interaction with cancer cells.

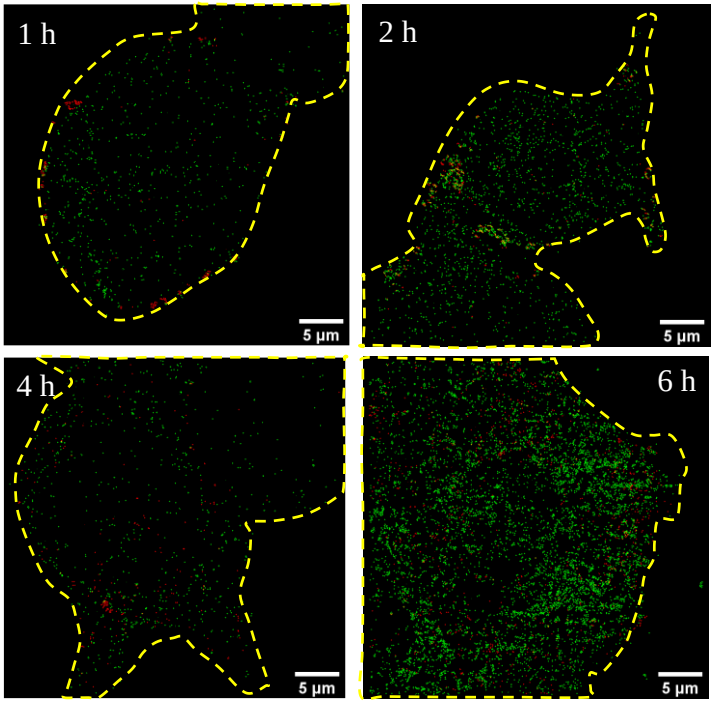

Figure S56. The evaluation of time-dependent cellular uptake of oriented antibody conjugated ESC4 nanorods (EAB4H) by prostate cancer LNCaP cells using dSTORM imaging, indicating localization of nanoparticles on the cell surface at the early stage (i.e., 1 h) and after long time incubation (i.e., 6 h), the nanoparticles become located in the cell cytoplasm. The green and red colors represent the nanoparticle and antibody, respectively.

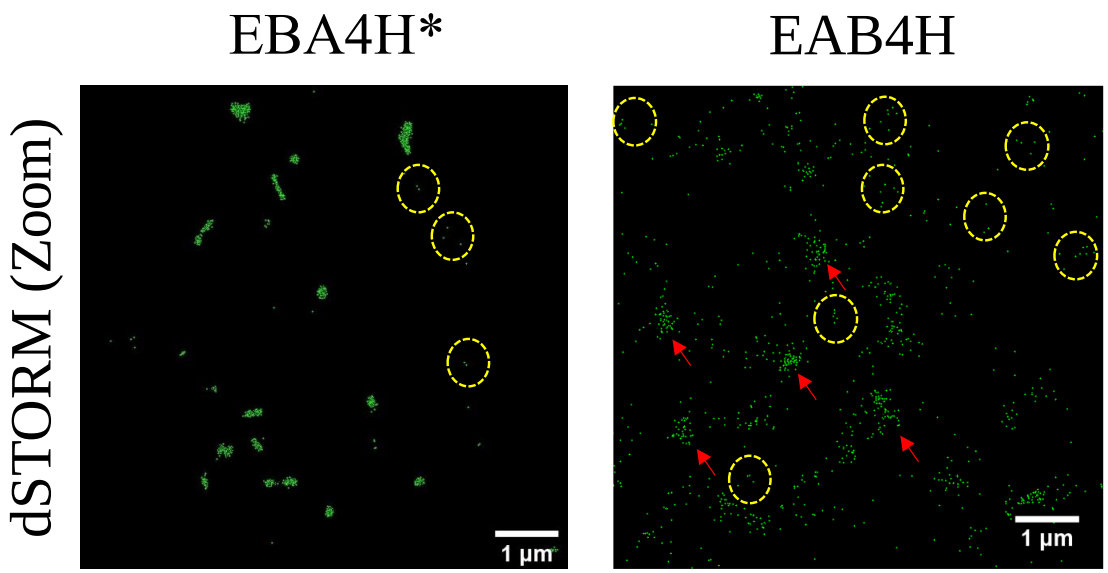

Figure S57. dSTORM images in zoom mode of prostate cancer LNCaP cells labeled with antibody conjugated nanoPMOs nanorods. The typical diffusion of Cy3 dye blinking from nanoPMOs and subsequent the production of low-numbered localizations from released Cy3 dye molecules are marked by red-colored arrows and yellow-colored circles, respectively.

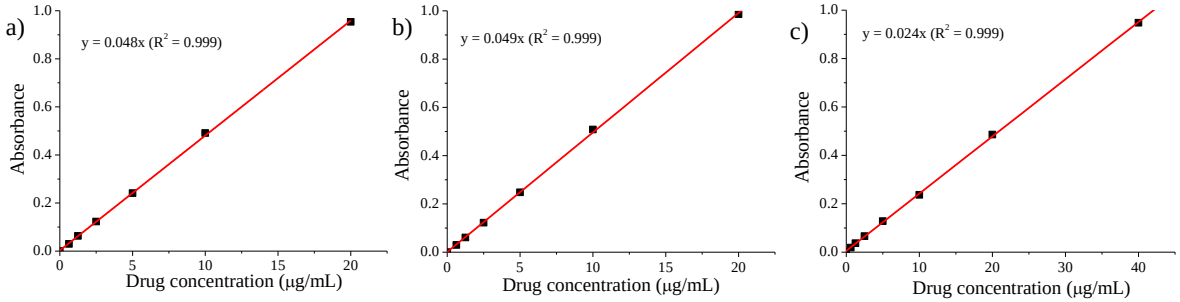

Figure S58. Calibration curves of different anticancer drugs a) 5-fluorouracil, b) gemcitabine hydrochloride, and c) doxorubicin hydrochloride in 10 mM phosphate buffer (pH 7.4) for quantification of drug loading in various functionalized nanoPMOs. The absorbance of 5-fluorouracil, gemcitabine hydrochloride, and doxorubicin hydrochloride was examined at 267 nm, 268 nm, and 490 nm wavelengths, respectively.

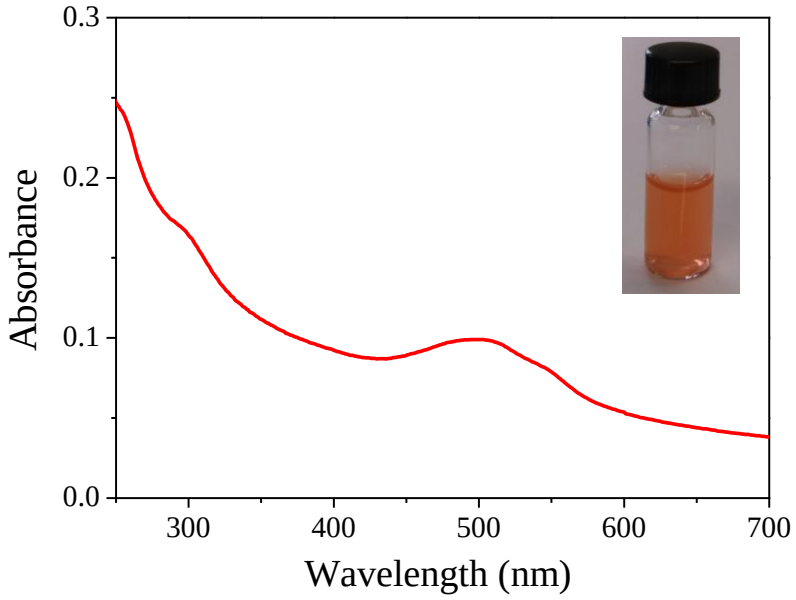

Figure S59. UV-visible absorbance spectrum of an aqueous solution of doxorubicin loaded oriented antibody conjugated ESC4 nanorods (EAB4H). The inset shows the corresponding solution at high concentration.

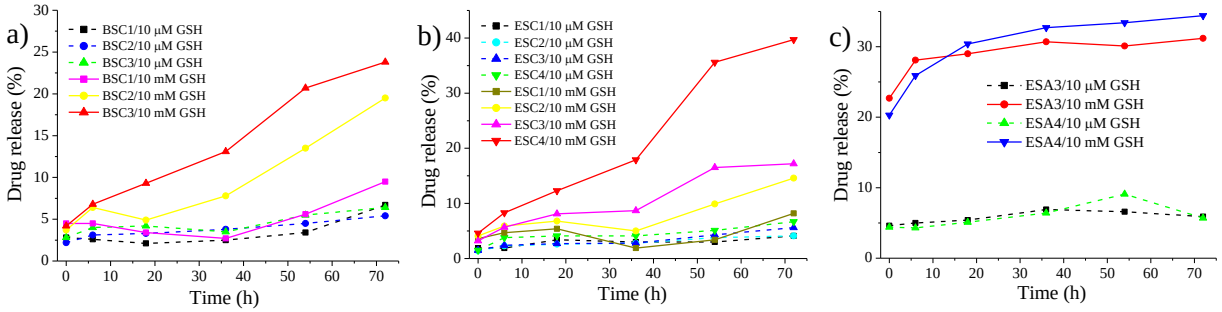

Figure S60. *In vitro* glutathione responsive drug release profiles of doxorubicin (DOX) loaded various functional nanoPMOs at physiological pH 7.4 and room temperature in 10 mM phosphate buffer solution of glutathione (GSH) at different concentrations. Time dependent DOX release from a) semicarbazide functionalized spherical nanoPMOs, b) semicarbazide functionalized nanoPMO nanorods, and c) carboxyl acid functionalized nanoPMO nanorods incubated with 10 μM and 10 mM GSH solution.

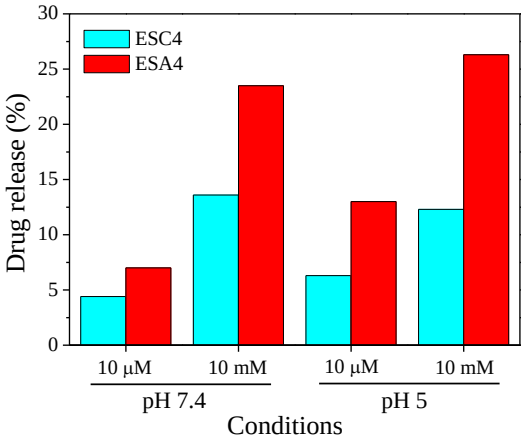

Figure S61. The quantification of released doxorubicin from drug loaded ESC4 and ESA4 nanorods after 24 h incubation at different glutathione concentrations and pH.

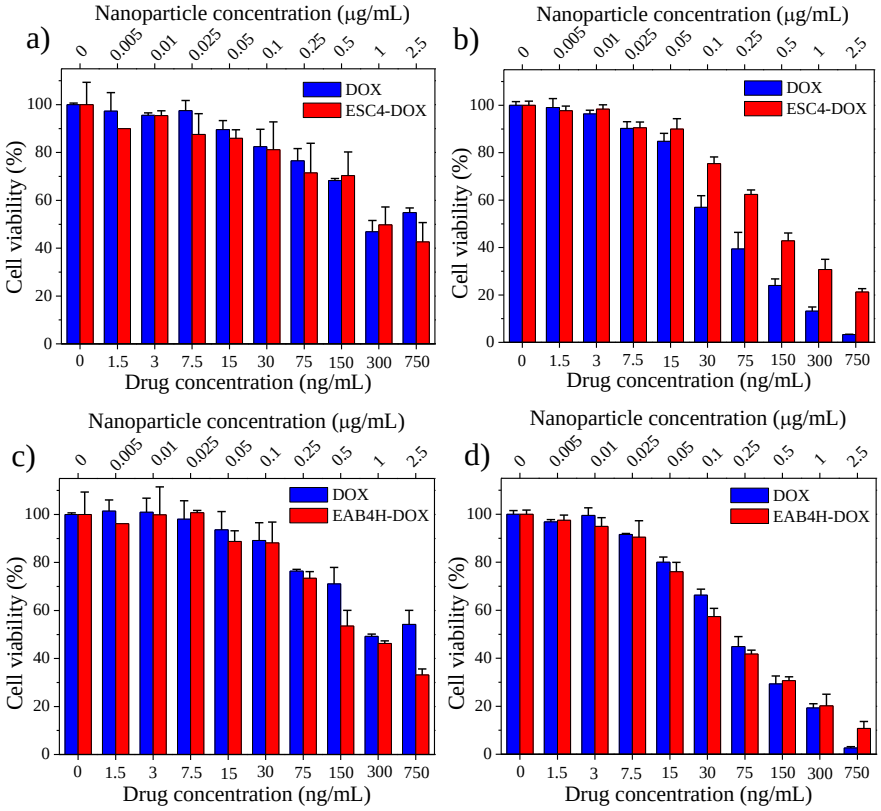

Figure S62. a, b) *In vitro* cytotoxicity of free doxorubicin (DOX) and doxorubicin loaded ESC4 nanorods (ESC4-DOX) against human prostate cancer LNCaP cells after 24 h and 48 h incubation, respectively at different drug and nanoparticle concentrations. c, d) *In vitro* cytotoxicity of free doxorubicin (DOX) and doxorubicin loaded oriented antibody conjugated ESC4 nanorods (EAB4H-DOX) against human prostate cancer LNCaP cells after 24 h and 48 h incubation, respectively at different drug and nanoparticle concentrations. Data are presented as mean ± SD of three independent experiments.

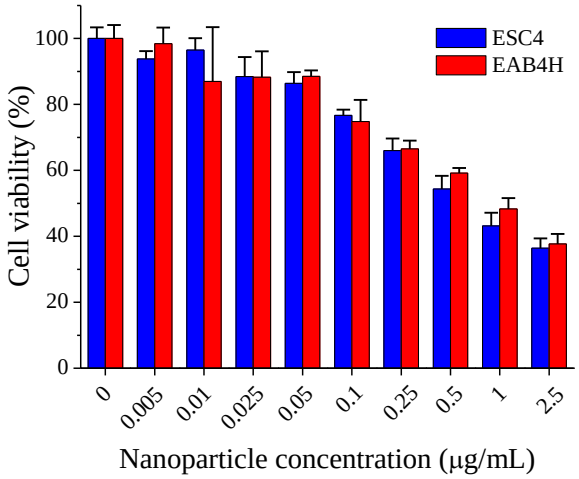

Figure S63. *In vitro* cell viability of human prostate cancer LNCaP cells incubated with pristine ESC4 nanorods and oriented antibody conjugated ESC4 nanorods at high density (EAB4H) at different nanoparticle concentrations for 72 h. Data are presented as mean ± SD of three independent experiments.